8-2002

Design and Analysis for Melt Casting Metallic Fuel Pins Incorporating Volatile Actinides

Xiaolong Wu
University of Nevada, Las Vegas

DESIGN AND ANALYSIS FOR MELT CASTING METALLIC FUEL PINS INCORPORATING VOLATILE ACTINIDES

by

Xiaolong Wu

Bachelor of Science
Nanjing University of Aeronautics & Astronautics
1998

Master of Science
University of Nevada, Las Vegas
2002

A thesis submitted in partial fulfillment of
the requirement for the

Master of Science
Department of Mechanical Engineering
Howard R. Hughes College of Engineering

Graduate College
University of Nevada, Las Vegas
August 2002

UNLV

UNIVERSITY OF NEVADA, LAS VEGAS

Thesis Approval

The Graduate College
University of Nevada, Las Vegas

May 31 , 2002

The Thesis prepared by

Xiaolong Wu

Entitled

Design and Analysis for Melt Casting Metallic Fuel Pins Incorporating Volatile Actinides

Students Attending the University of Nevada, Las Vegas

is approved in partial fulfillment of the requirement for the degree of

Master of Science in Mechanical Engineering

Examination Committer Chair

Examination Committer Chair

Examination Committee Member

Examination Committee Member

Graduate College Faculty Representative

ABSTRACT

Design and Analysis for Melt Casting Metallic Fuel Pins Incorporating Volatile Actinides

by

Xiaolong Wu

Dr. Darrell W. Pepper, Examination Committee Co-Chair
UNLV, Professor of Mechanical Engineering

Dr. Yitung Chen, Examination Committee Co-Chair
UNLV, Associate Professor of Mechanical Engineering

Fundamental issues related to the selection of a metallic fuel casting furnace design are presented and discussed including heating mechanisms, casting issues, crucible design, and issues related to the mass transport of americium. The process of evaluating all of these different criteria is undertaken to select a concept that would have the greatest chance of success for casting americium in a metallic fuel rod. Based on this evaluation process, a concept for the casting of metallic fuel pins containing high vapor pressure materials is selected and discussed. The important physics of this concept include mass transport of americium from the melt, induction heating and stirring of the melt, plus casting of long slender fuel rods. This work shows process of evaluating important steps of casting fuel rods. A discussion of the preliminary modeling results for the casting of long, slender fuel rods will be presented. The model considers the flow of the melt into the molds, heat transfer into molds, and the impact of process parameters on the formation of the fuel rod. Collection of properties of volatile actinides is also discussed.

LIST OF FIGURES

LIST OF TABLES

ACKNOWLEDGEMENTS

Considerable amounts of time were used to track the related information about the casting furnace conceptual design and run the FIDAP code to simulate the filling process. In this research, grand support for this work was funded from AAA-UPP program. Technical support associated with the background information and some useful materials data was provided by the Argonne National Laboratory-West. I need to give a very special thanks to my advisors Dr. Yitung Chen, Dr. Darrell Pepper and Dr. Randy Clarksean for the support and directions they gave me on this undertaking.

CHAPTER 1

INTRODUCTION AND BACKGROUND

1.1 Nuclear Waste

Fission occurs when atoms split and cause a nuclear reaction. Nuclear waste is produced whenever nuclear fission takes place and high-level radioactive waste is a by-product of making electricity at commercial nuclear power plants. It also comes from nuclear materials produced at defense facilities. Nuclear waste is predominately comprised of used fuel discharged from operating nuclear reactors. [1]

In the United States, the roughly 100 operating reactors (which currently produce about 20% of the nation's electricity) will create about 87,000 tons of such discharged or "spent" fuel over the course of their lifetimes. Sixty thousand tons of this waste is destined for geologic disposal at the Yucca Mountain site in Nevada, along with another ~10,000 tons of so-called defense waste. Worldwide, more than 250,000 tons of spent fuel from reactors currently operating will require disposal.

These numbers account for only high-level radioactive nuclear waste generated by present-day power reactors. Nuclear power could develop so quickly by year 2050, that almost 1 million tons of discharged fuel - requiring disposal, could exist. All of these depend on how to handle the waste to improve the safety and environment concern. [2]

1.2 Transmutation Technology

Because the spent nuclear fuel contains unstable nuclei in sufficient quantities to render the material hazardous for a prolonged period of time, the process of disposing of the spent nuclear fuel is important. Any storage scenario would want to isolate these materials from the environment for a period somewhere between 10,000 to perhaps a million years. This long period challenges human being's abilities of design long-lasting containers and barriers, and therefore forces some reliance on predictions of geologic behavior to assure the required long-term isolation from the environment. These predictions are very complicated and have the potential to have large uncertainties. [2]

Nuclear waste transmutation is an option that arises when one examines the hazardous components in the spent nuclear fuel. The long-term hazards are posed by about 1% of the content of the spent fuel, which include the plutonium, neptunium, americium, curium, iodine, and technetium, leaving the other 99% relatively harmless over the long term. After we applied transmutation technology, the isotopes that are present in the problematical 1% can be converted to either stable or short-lived hazards when exposed to neutrons in an appropriate energy range. Finally, most of the materials in the 1% (the transuranics) will fission, releasing large amounts of energy. [2]

Normally transmutation is defined as nuclear transformation and describes processes that have occurred naturally since the origin of the universe. Radioactive dating of fossils is based on a measurement of the natural decay of carbon-14 to nitrogen, reflecting the amount of transmutation that has occurred over time. Transmutation occurs every time the nucleus of an atom changes as a result of natural radioactive decay, nuclear fission, nuclear fusion, neutron capture, or numerous other processes. [2]

There are three major benefits that can result from transmuting these hazardous waste components. First, we can greatly reduce the amount of long-lived hazardous materials. Transmutation also reduces the need to attempt to provide control of geologic (and climatic) behavior in the future, shifting the isolation burden into the time frame of man-made containers and barriers. Secondly, the partitioning and transmutation process allows for the use of optimized waste forms, which can be made highly resistant to leaching and other natural processes. Leaching or other transport processes, might transfer the hazardous materials into the groundwater supply. Finally, by transmuting most of the transuranics, such as actinides, one greatly reduces any incentive for future generations to re-enter (or mine) the repository. [2]

1.3 Advanced Accelerator Application Program

The Advanced Accelerator Application (AAA) Program is to improve the current nuclear waste processing technology; so that there is less concern over the management of the nuclear waste produced by nuclear power plants. The AAA program is developing a technology base for nuclear waste transmutation, which researchers hope can transform long-lived radioactive materials into short-lived or non-radioactive materials. Efforts are also being made to demonstrate its practicality and value for long-term waste management. AAA's transmutation technology has the potential to extract energy from nuclear waste and make it available to the national power grid, representing a potentially huge amount of energy (Equivalent to ~10 billion barrels of oil). Another troubling issue is the decline of engineers or scientists with a nuclear background. Since 1980, nuclear engineering enrollments at US universities have sharply declined. No new nuclear power

plants have been ordered in the United States since the late 1970s. Although the US retains considerable influence in global nuclear issues due to its superpower status, its relevance and leadership in the international arena of nuclear technology is shrinking substantially. The AAA program plans to construct an advanced accelerator-driven test facility that will provide unique and flexible capabilities for demonstration of nuclear waste transmutation and advanced nuclear technologies such as those for Generation IV reactors (solving electricity shortage and current electricity generation environmental contamination.). The AAA program will establish and support a national university program to reenergize development and training in nuclear engineering and related fields, and develop research partnerships to rebuild a declining national nuclear science technology base. [2]

1.4 Safety Characteristics and Fuel Manufacturing Process

Advanced reactors of the future might be even safer than the current generation of nuclear power plants. This additional margin of safety can be achieved by designing plants to enhance "passive" safety characteristics and active safety systems in use today. In technical jargon, a passive safety characteristic is determined by the laws of nature, and does not rely on the proper functioning of human operators or special equipment.

Basically, accidents can only result from failures in which more heat is produced in the fuel than is carried away by the coolant. If the fuel gets hot enough, radioactive fission products will be released from the fuel because the cladding ruptures or melts. Radioactivity would still be kept away from the environment by the steel reactor vessel and the large containment dome. Only a small amount of inert radioactive gas could be

released. But the psychological effect of the accident on the local population can be traumatic, and the cost has been staggering. Clearly, there is a strong incentive to design power stations such that upsets in the plant are much less likely to lead to a reactor accident. This incentive has led to substantial improvements in today's nuclear plants, but exciting work is also being done to optimize the inherent safety features of future reactors. [3]

Metal fuel was crucial to the improved safety characteristics of the Integral Fast Reactor (IFR), as well as to a new and much simpler fuel cycle technology. Most reactors today use a ceramic fuel, generally uranium oxide. Compared to oxide, metal fuel has thermal conductivity about ten times higher than that of the ceramics (ceramics are usually thought of more as insulators, rather than conductors, of both electricity and heat). With high thermal conductivity, the heat generated by fission within the fuel slug is transferred to the coolant more effectively, resulting in a much lower temperature in the center of the fuel. This is a major safety advantage. Abnormal reactor conditions involving loss of coolant flow into the reactor core can be accommodated with little or no damage of any kind, even if normal safety systems fail to function. [4]

The casting process to produce these fuel metallic rods, will be briefly discussed here. First, molds-straw-like tubes with one end closed, are prepared for the casting. Quartz glass molds are used because it will not soften or distort when filled with molten metallic fuel. The inside of each mold is first coated with a high temperature ceramic paint. These molds are then loaded into a pallet. Then the pallet is taken to the furnace room for the fuel casting operation. Meanwhile, the feed-stock - consisting of end pieces from previously cast fuel slugs, leftover fragments from previous casting, rejected slugs, and

fresh feedstock (including actinides, americium, plutonium and zirconium) - are loaded into the crucible. The furnace and its enclosure prevent release of particulates into the atmosphere, maintaining a clean environment in the hot cell. The furnace basically consists of an area for the molds and another for the crucible containing the feedstock. An induction heating technique is used to heat the materials in the crucible. Between the crucible and coil is a layer of zirconium oxide insulation to prevent large heat losses from the crucible and to keep the induction coil cool. The mold pallet is positioned above the crucible until the fuel is molten and ready for injection casting. The furnace system is then ready for the direct melting of the raw and recycled materials for casting the fuel to final dimensions.

Traditionally, high concentration uranium, plutonium zirconium fuels were manufactured. For the AAA program, the fuels of interest need to consider including americium, plutonium, and zirconium. Americium has a low vapor pressure and is a major concern from a processing standpoint.

As the crucible heats up, the casting charge is heated and melts. The melt is then magnetically stirred to assure homogeneity of the melt before casting. When the proper temperature is reached, the system is evacuated by a vacuum pump. The molds are then submerged into the melt, the unit is pressurized, and the molten fuel is injected into the evacuated molds. This takes less than a second. Once filled, the molds are withdrawn from the remaining melt and cooled - producing about a hundred metallic fuel pins - all in one operation. This one-step fabrication process has many advantages, such as yields are high. Recycle material is easily used in subsequent castings. The cost is low because the process is simple, straightforward, and flexible. After casting, the quartz molds

containing the solidified fuel slugs are removed from the furnace for processing. The slugs are remolded and mechanically sheared to length. Next, they are sampled for chemical analysis, measured, and weighed. The fuel slugs are enclosed in stainless steel jackets for use in the reactor. Sodium to fill the space between the fuel slug and the jacket is extruded, measured, and placed in the jacket first. The jacket is heated in a low-temperature furnace to melt the sodium. Then the slugs are lowered into the jacket and allowed to settle to the bottom. The liquid sodium fills the space between the fuel slug and the inside wall of the jacket.

Each fuel element is x-rayed and inspected for weld quality and bond integrity. The sodium level is checked, and the fuel structure is inspected for defects. The final assembly is simple and straightforward. The elements are loaded on to a hexagonal grid, placed into a hexagonal shaped can, and welded. [3]

1.5 Purpose of Study

An important aspect of the Advanced Accelerator Application (AAA) program is the development of a casting process by which volatile actinide element (i.e., americium) can be incorporated into metallic fuel pins. The traditional metal fuel casting process used inductively heated quartz rods as fuel pin molds. Once evacuated the open ends of the molds are lowered into the melt; the casting furnace is then rapidly pressurized, forcing the molten metal up into the evacuated molds where solidification occurs.

This process works well for the fabrication of metal fuel pins traditionally composed of alloys of uranium and plutonium, but does not work well when highly volatile actinides are included in the melt. The problem occurs both during the extended time

period required to superheat the alloy melt as well as when the chamber must be evacuated. The high vapor-pressure actinides, particularly americium, are susceptible to rapid vaporization and transport throughout the casting furnaces, resulting in only a fraction of the charge being incorporated into the fuel pins as desired. This is undesirable both from a materials accountability standpoint as well as from the failure to achieve the objectives of including these actinides in the fuel for transmutation. [5]

It order to solve above problem, three steps will be carried out as follows. The first step would include the study, analysis and selection of a new casting furnace design. Second would lead to the fabrication of a scale furnace design at UNLV to demonstrate the proposed furnace concept using nonradioactive surrogate materials. Additional analysis work would be conducted during this time to validate the modeling efforts and to support the testing program. And detailed modeling to make detailed comparisons to the experimental test results will be used to assist in the system design. Then surrogate non-radioactive materials will be selected to perform a series of tests. Finally, using actinide elements to demonstrate the acceptable use of the new furnace in a simulated remote environment.

In my thesis, mostly focus is on the first step of this project: study, analysis and selection of a new casting furnace design. All the mechanism and furnace options are considered: heating mechanisms, casting issues, crucible design and issues related to the mass transport of americium. The evaluation process is undertaken to select a concept that should have the greatest chance of success for casting americium into a fuel pin. Then one of the basic phenomena that exist in the proposed furnace is studied: the flow of melt into the chill molds and heat transfer into the molds. This thesis presents some

preliminary modeling results for the casting of long, slender fuel rods. The model considers the flow of the melt into the molds, heat transfer into the molds, and the impact of process parameters on the formation of the fuel rod.

CHAPTER 2

FURNACE SELECTION

Before select a melting casting process, the following issues need to be considered: heating mechanisms, casting issues, crucible design, and issues related to the mass transport of americium. Figure 2.1 schematically shows all these fundamental issues during the selection of the casting process.

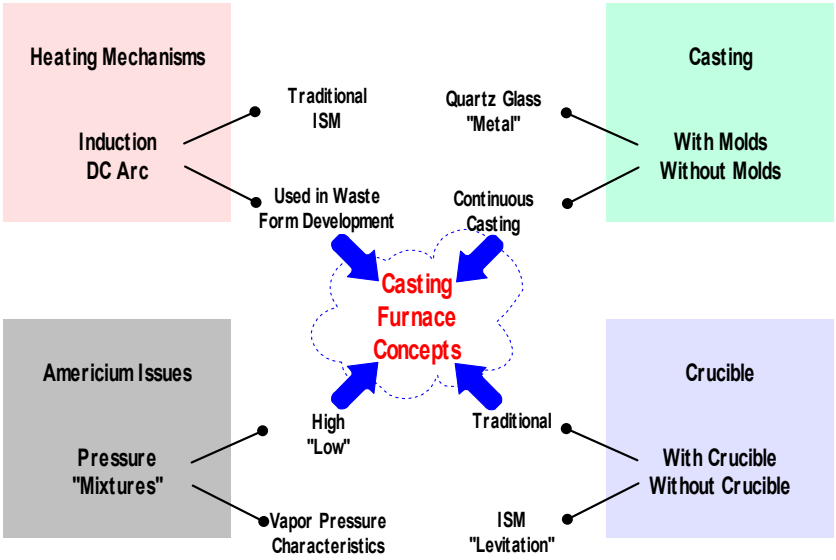

Figure 2.1 Outline of mechanisms and furnace options evaluated in the design process

Usually there are two heating methods: induction heating and DC Arc heating. Induction heating processes are widely used in industrial manufacturing, including metal melting, crystal growing, semiconductor wafer production and heating of metallic

surfaces. At high temperatures the most practical method to heat crucibles is by electromagnetic induction. Induction heating has been defined as occurring in an electrically conducting object, not necessarily magnetic steel, when the object is placed in a time varying magnetic field. The induction coil induces an alternating current that flows through the crucible. The Ohmic resistance encountered by this current dissipates energy, thereby directly heating the crucible or materials via internal heat generation. In an induction heating application, as in a microwave, there is no physical contact between the energy source and the product being heated. [6]

Induction heating can bring a piece of steel to austenitizing temperatures in a fraction of the time required by conventional methods. This rapid heating action dramatically lowers the time at elevated temperature. It is also possible with this method to heat steel to higher temperatures than practical in conventional equipment, allowing for new materials to be successfully heated. This becomes particularly important when heat treating materials such as chrome silicon, chrome vanadium, or similar alloys that are known to be difficult to properly heat treat. It is also possible to have intense stirring of molten material in the crucible as a result of the inducted field, which results in high alloy uniformity. This can be controlled by adjusting the numbers and position of the induction coils, along with the frequency of the electrical field in the coils. [7]

A number of industries also use DC Arc heating. There may be one or more electrodes. Here the charge is heated by means of an electric arc produced between opposed electrodes (indirect arc furnaces) or between an electrode and the charge (direct arc furnaces). Using DC Arc heating can achieve high temperatures and lower

maintenance costs. The graphite electrodes do not have to be cooled compared to metal electrodes. [8]

Short DC arcs are effective in transferring thermal energy into the materials to be processed. But the high temperature region around the arc (gases may be exposed to the arc temperature) will destroy organic species and vapors that evolve from the material being processed. [9][10]

The fuel rods can be formed through the use of molds or continuous casting. Argonne National Laboratory (ANL) has extensive experience in using molds for casting, but this approach does produce a waste stream, the shattered quartz glass rods. In addition, it requires rapid pressurization and possibly some preheating of the molds. [11] Continuous casting means the solidified shape of the rod is produced as it leaves a mold region. It may be difficult to control the tight tolerances necessary to make fuel rods through the use of this technique.

Many traditional casting furnaces have a crucible for containing the molten material. Other furnaces, such as the induction skull melter, do not rely on a traditional crucible. The “crucible” in the induction skull melter is the “skull” of material formed within a set of copper molds that are internally cooled. This cooling process forms a crucible region referred to as a “skull” region. [12][13] The contamination of molten metal by tramp elements which form the crucible which is made of refractory materials and the reaction between metal and crucible make it difficult to produce high purity. There are some materials which have higher melting points than the crucible materials. For these reasons, a new casting method, levitation melting has been developed to resolve these difficulties. [14]

In this situation, magnetic fields are used to maintain molten fluid within a specified region. [15]

The last mechanism deals with factors that can impact the transport of americium. The pressure could be increased to deter the evaporation of americium.

An evaluation process was undertaken to select a concept that should have the greatest chance of success for casting americium into a fuel pin. After several sessions with the assistance of ANL-West staff, six conceptual designs were developed. [16] [17] [18] [19] [20] [21]

They are:

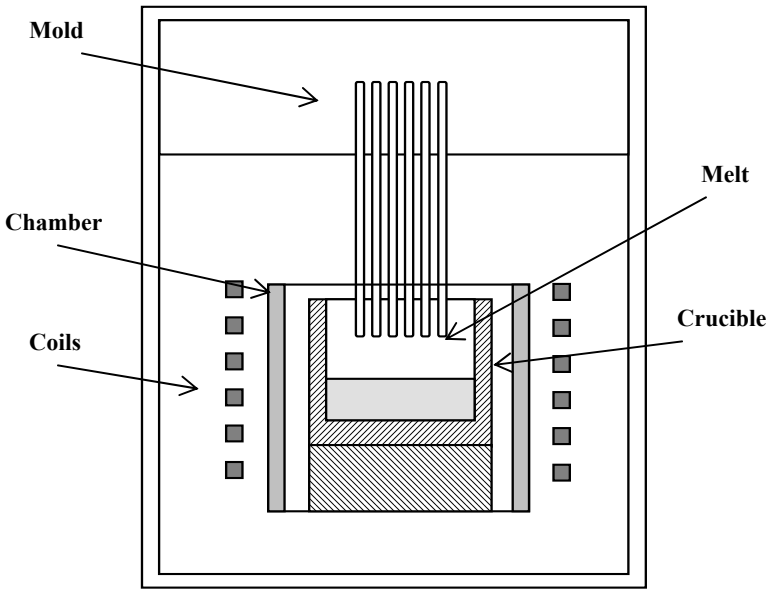

Figure 2.2 Inductively heated pressurized chamber vacuum cast (molds)

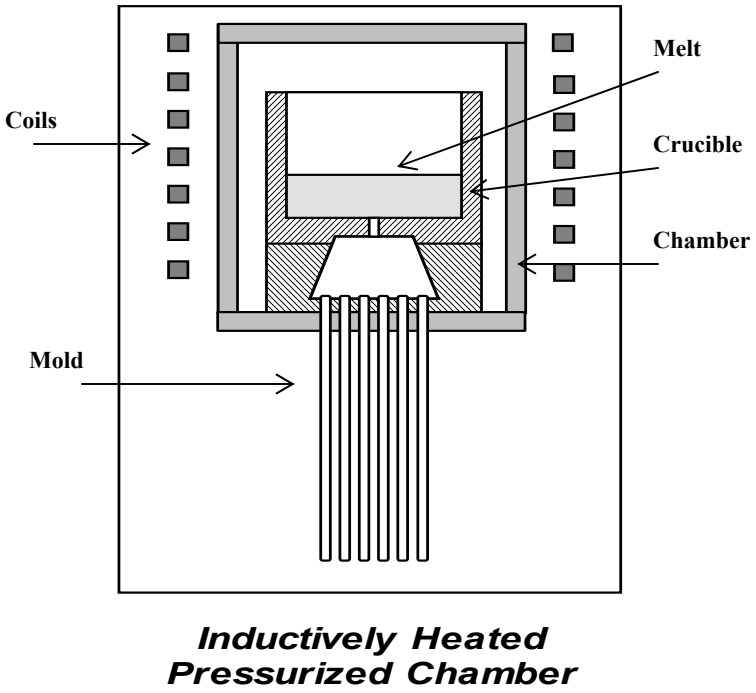

Figure 2.3 Inductively heated pressurized "local" chamber

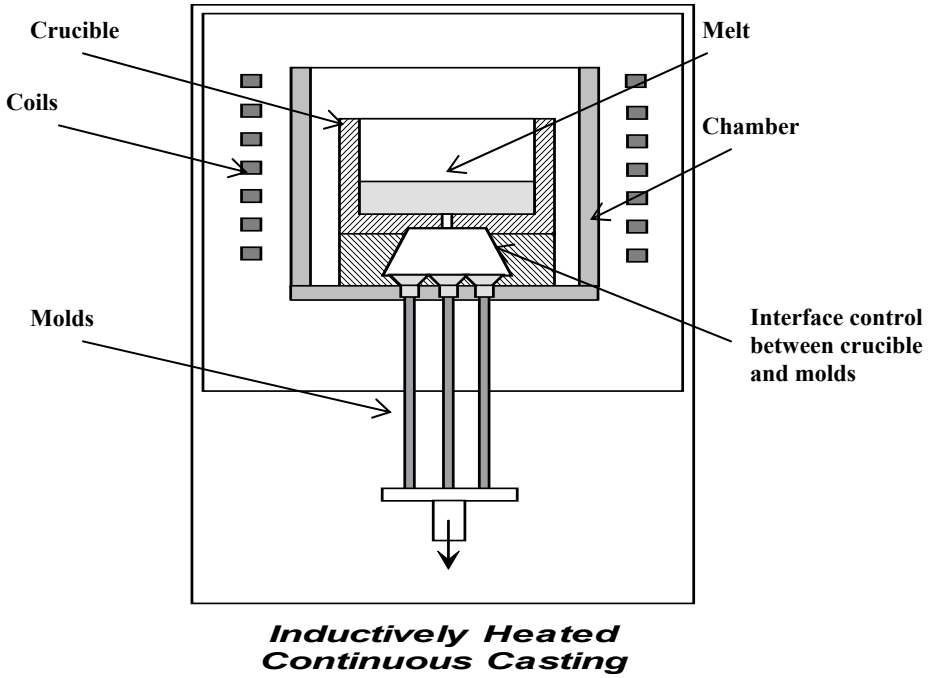

Figure 2.4 Inductively heated continuous casting

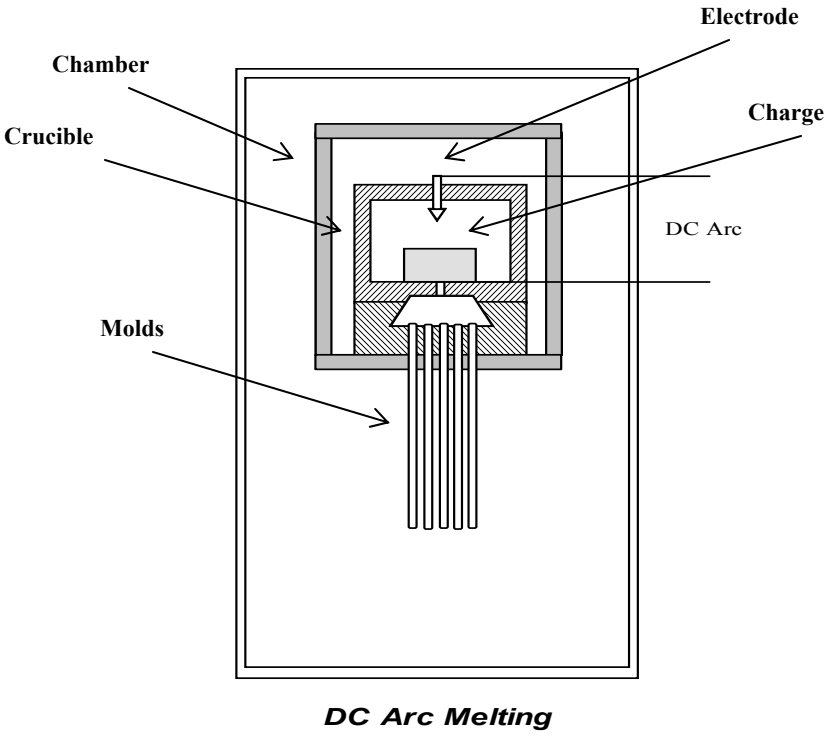

Figure 2.5 DC Arc melting with pressurized/gravity molds

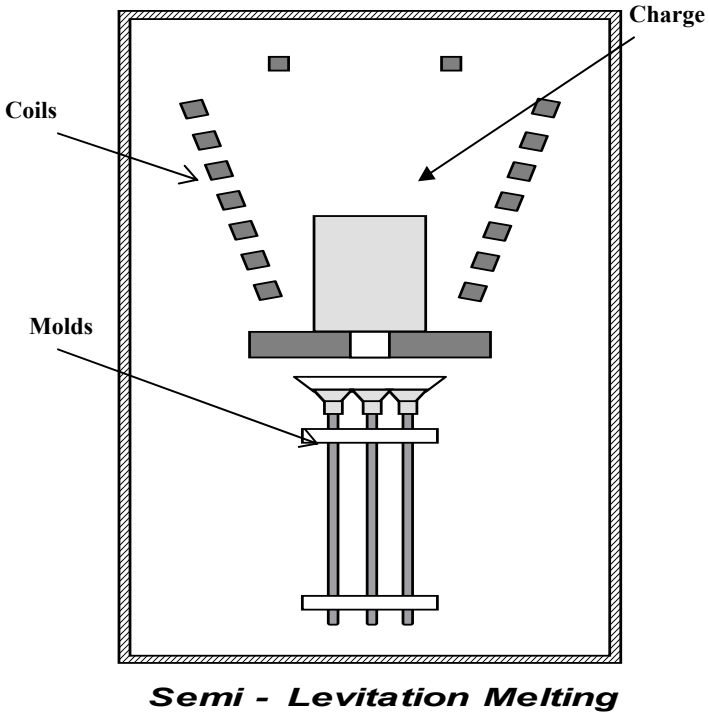

Figure 2.6 Semi-levitation melting

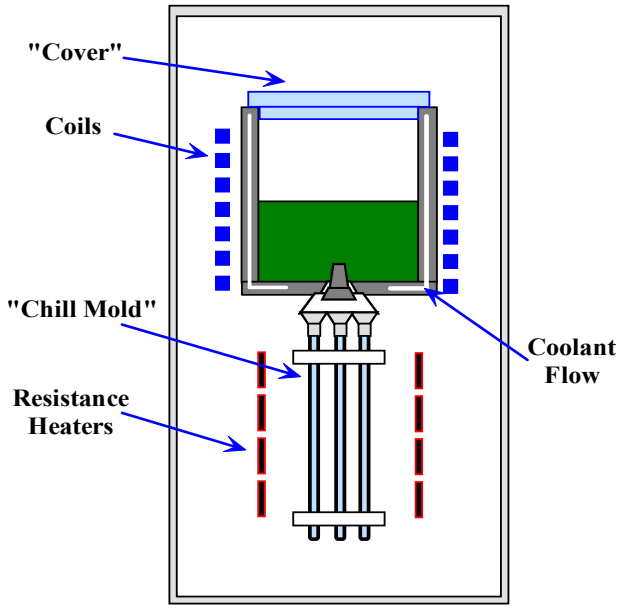

Figure 2.7 Induction skull melting (ISM) with pressurized/gravity molds

Figure 2.2 illustrates the Inductively heated-pressurized/vacuum molds. This model uses induction heating. After the charge was heated and melts, then it will be magnetically stirred to make sure the homogeneity of the melt. When the proper temperature is reached, the system is evacuated by a vacuum pump. The molds are then submerged into the melt, the unit is pressurized, and the molten fuel is injected into the evacuated molds. Once filled, the molds are withdrawn from the remaining melt and cooled - producing about a hundred metallic fuel pins. Currently, ANL-West has a lot of experience with this type of design. The control of the americium transport would be done with changes in pressure. Molds are still needed. It is uncertain whether or not long slender rods could be cast with this approach (~1 m length). Shorter segments would possibly have to be cast. Shorter segments could be cast and used in the fuel rod/element if one long fuel pin cannot be cast. The rapid pressurization of molds complicates the

design. The higher pressure also leads to more involved pressure vessel (chamber) design issues.

Figure 2.3 represents an inductively heated pressurized “local” chamber furnace. This model has a small, heated and pressurized “local” chamber, which is better for controlling americium transport. The molten fluid flows into the molds by gravity or through rapid pressurization. This concept still needs molds-the molds would still need some type of preheating to cast a long slender rod. It would be hard to control the rod temperature and maintain some type of pressurization in the “covered” crucible area. Deposition and transport of americium from the crucible would likely occur by pressure.

Figure 2.4 shows the inductively heated continuous casting furnace. Conduction heating is used to heat the charge. Again, this system can be pressurized to decrease americium transport. Continuous casting would be used to cast the rods of desired length. The control of rod dimensions could be difficult for remote fabrication in a hot-cell environment. The design of the continuous casting process is complex and might be difficult to control remotely. This process will have a longer duration casting time, which leads to increased americium losses because the melt is exposed to for a longer period of time.

The DC arc melting with pressurized/gravity molds furnace is shown in Figure 2.5. This concept uses DC arc to heat the charge causing the melt to flow into the molds by gravity or through pressurization. This model only use one electrode, so from an economics standpoint, it will save energy. DC arc heating can deal with a wide range of materials, including metals, nonmetals, and contaminated soil, etc. DC arc heating will

generate a high local temperature, which could lead to rapid vaporization of americium-which is not our preferred design goal.

The concept in Figure 2.6 considers a semi-levitation melting furnace. Semi-levitation does not use a crucible. When the charge is heated by induction coils, it will then melt and flow into the molds by gravity. It can produce a high purity melt, which is better for some reactive metal alloys. This system is limited by the amount of levitated mass. It could be successful in microgravity conditions. The heating of the melt is a dynamic process, which will cause more americium loss. More exposed surface will also cause more americium loss. A complex design for the chamber would also be needed. [10]

Figure 2.7 is the final selection about the casting furnace design, which shows a schematic of the proposed furnace design to cast metallic fuel pins that contain americium. The primary difference between the ISM and other casting options is the nature of the crucible. The crucible is a slotted, cooled copper design. Great melting efficiencies could be achieved by splitting the crucible into a multi-segments crucible. Also the increased number of crucible segments renders the crucible discontinuous enough to levitate the melt sufficiently to prevent excessive arcing and resulting crucible damage. The oxygen and nitrogen contamination during the melting process is also eliminated due to the skull crucible. The crucible cover was selected to aid in controlling the transport of americium from the melt. The resistance heaters were added to insure that preheating of the molds could be controlled to insure the melt will flow into the molds. In ISM, the induction fields and constant intense stirring of metal maintain a high level of superheat throughout the melt, so the temperature of the initial metal poured is virtually identical to the temperature of the final metal poured from a heat and a high

purity melt can be achieved. Chill molds were selected over continuous casting to insure proper geometric control. The melt will flow into the molds either by gravity or through pressurization. These two cases are simulated to see which one is better. The copper molds and quartz molds options are also analyzed to determine a better selection.

CHAPTER 3

PHYSICAL AND NUMERICAL MODEL

First, the details of the physical model and the simplifying assumptions will be presented. Second, governing equations for the numerical model will be presented. These equations are solved using a commercially available finite element method solver FIDAP (Fluid Dynamics Analysis Package). VOF (Volume of Fluid) and parametric study will then be discussed and studied.

3.1 Description of Physical Model

As shown in Figure 2.7, the general geometry of the induction skull melter (ISM) furnace consists of an induction skull melter, a crucible cover, "chill" molds and resistance heaters. The crucible cover will be helpful to control the transport of americium from the melt. Chill molds were selected over continuous casting to insure proper geometric control. We use resistance heaters to control the molds preheating temperature, which makes sure the melt will flow into the molds.

Several basic phenomena exist in the proposed furnace and need to be analyzed. These phenomena include:

- Transport of americium from the melt into the upper regions of the crucible region.

- Impact of induction heating on the flow and heating of the melt material, and
- The flow of melt into the chill molds.

This thesis addresses this last phenomenon, the flow and heat transfer associated with the melt entering the chill molds. The important physics of this process includes

- Heat transfer from the melt into the mold,
- Mold size, shape and material,
- Preheating of the molds,
- Mechanism to force the flow into the molds (pressure injection vs. gravity), and
- Phase change characteristics of the melt.

As the crucible heats up, the plutonium, americium, and zirconium feedstock melts. The melt is then magnetically stirred to assure homogeneity of the melt before casting. When the proper temperature is reached, the melt will flow into the molds. A number of different velocities will be assumed to study how rapidly the melt must flow into the molds in order to prevent solidification prior to reaching the end of the mold. It is assumed that the melt flows out of the crucible and down into the molds.

Figure 3.1 shows the geometry of the mold model with one end closed. The total length of the mold varies in the simulations, but ranges from 0.5 to 1.0 meter to find what range of length we can have low americium loss. The inner radius of the mold is 4 millimeters and the outer radius is 8 millimeters. Before the molten fluid fills into the molds, the molds are considered to be preheated. The molds are preheated to insure that the melt flows nearly the full length of the mold, giving the desired rod length.

The molds have a cylindrical shape which can be reduced to axi-symmetric geometry involving radial, axial components. Figure 3.2 shows the simplified geometry. The use of

this simplified geometry can reduce the computational times. The variables affecting

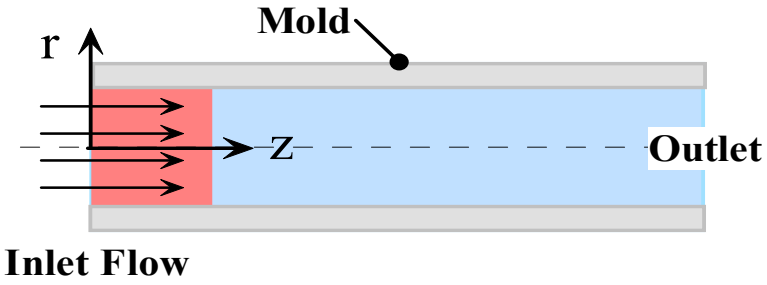

Figure 3.1 The schematic of fuel rod casting model

mold filling are the average fill velocity of melt, initial mold temperatures and the heat transfer coefficient between the melt and the mold. The filling process happens only within a few seconds. The heat transfer coefficient between the melt and the mold is an important factor affecting the heat transfer.

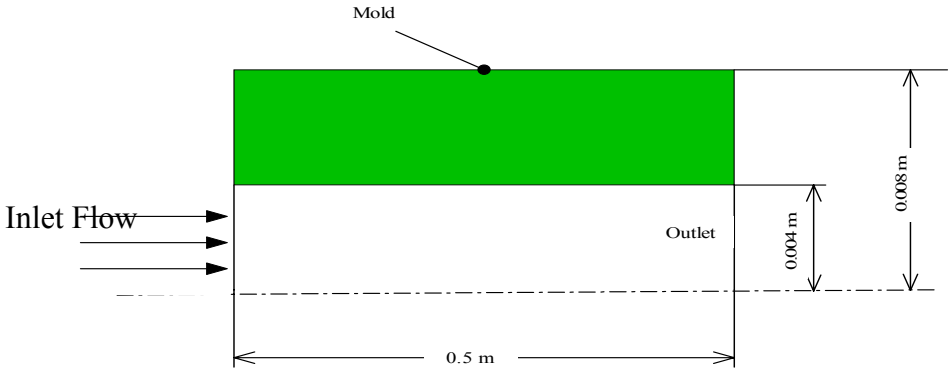

Figure 3.2 Geometry of fuel rod

3.2 Numerical Model

3.2.1 Governing Equations

The governing equations for the transient analyses of the melting of the phase change

material included the Navier-Stokes (momentum) equations, the continuity equation, and the energy equation. Figure 3.1 shows a schematic of the model, which includes the melt and the mold. The important physics of the problem include the heat transfer into the mold, cooling of the melt, thermal mass of the mold, and the necessary forces to cause the melt to flow into the mold. The cylindrical geometry to this mold can be simplified to an axisymmetrical geometry, which will reduce the computation efforts.

The problem will be analyzed numerically through the use of the commercial finite element package FIDAP™ (Fluid dynamic analysis package). This package is a general-purpose heat transfer and fluid mechanics code.

These equations are shown in tensor notation below. (All parameters are in the nomenclature.)

$$\rho \frac{\partial \vec{u}}{\partial t} + \rho(\vec{u} \cdot \nabla)\vec{u} = -\nabla p + \mu \nabla^2 \vec{u} \tag{1}$$

$$\nabla \cdot \vec{u} = 0 \tag{2}$$

$$\rho C_p \frac{\partial T}{\partial t} + \rho C_p \vec{u} \cdot \nabla T = k \nabla^2 T \tag{3}$$

Figure 3.3 shows the boundary and initial conditions for continuity and momentum equations. We assume the slow slipping along the mold inner wall, that will allow it to fill near the wall, which allow us to calculate the heat transfer from the melt materials into the molds. An initial constant filling velocity is also applied. Different initial filling velocity will be changed to represent different filling mechanisms, like gravity filling or

pressurized filling. There is no any kind of energy loss across the centerline of the molds.

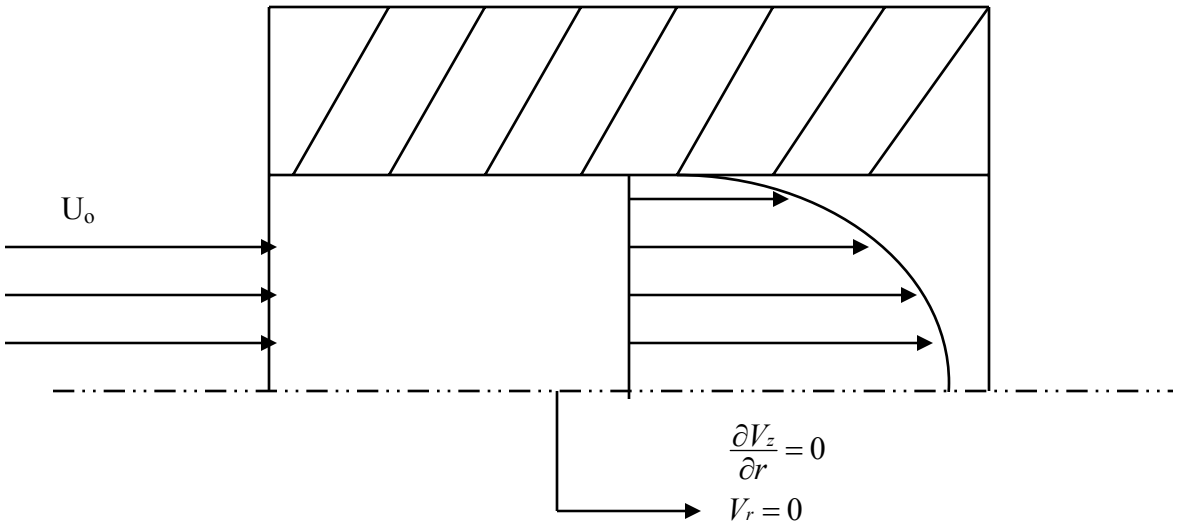

Figure 3.3 Boundary condition and initial condition for the continuity and momentum equation

Conduction within the solid (mold) required the solution of the conduction equation, which is shown below.

$$\rho C_p \frac{\partial T}{\partial t} = k \nabla^2 T \tag{4}$$

At the interface between the solid and the adjacent molten material, the conditions of

$$k_{mt} \frac{\partial T_{mt}}{\partial n} = h \cdot \Delta T = k \frac{\partial T}{\partial n} \tag{5}$$

equal temperature and energy conservation are required. The interface temperature does not have to match identically because a convective heat transfer relationship is used to model the interface between the melt and the mold. This technique is commonly used in casting analysis.

Figure 3.4 shows the boundary and initial conditions for the conduction equations in the molds and the energy equation. The initial melt filling temperature is 1500 ^{o}C. Because the filling time is less than one second and the small geometry of the molds, an adiabatic boundary condition was assumed here. The molds outer surface was initially kept as the initial preheating temperature.

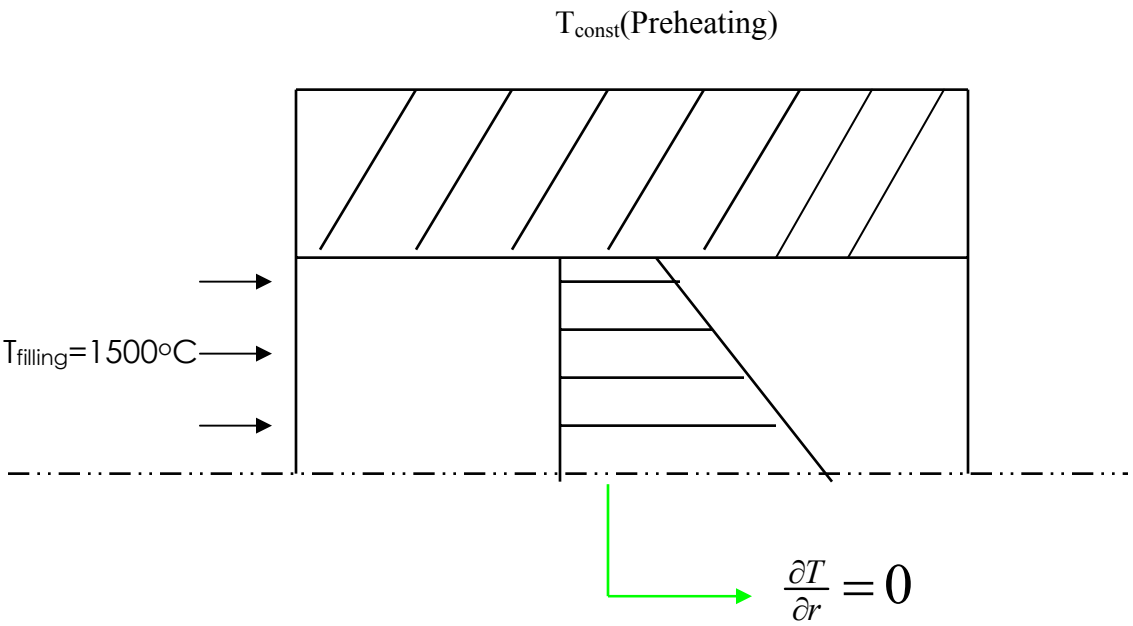

Figure 3.4 Boundary condition and initial condition for the interface and energy equation

3.2.2 FIDAP Solution

The finite element method (FEM) is a well-known numerical method. The interesting aspect of the finite element method is that the problem formulation results in a system of simultaneous algebraic equations instead of a system of differential equations. This is because a system or a body is modeled by subdividing into smaller elements. Finite element analysis involves the following steps, [22]

- Specify the geometry and divide domain into finite elements (small local regions where the governing equations are approximated)
- Formulate the properties of each element and determine the node properties using known information
- Assemble elements to obtain the finite element model of the domain
- Apply the known values – boundary and initial condition.
- Specify how the domain is affected by the known nodes
- Solve simultaneous linear algebraic equations to determine node transport properties (temperature, velocity, pressure, etc)

The power of the finite element method resides principally in its versatility. The method can be applied to various physical problems. The body analyzed can have arbitrary initial and boundary conditions. The mesh can mix elements of different types, shapes, and physical properties. This great versatility is contained within a single computer program. User-prepared input data controls the selection of problem type, geometry, boundary conditions, and element selection. Another attractive feature of finite elements is the close physical resemblance between the actual system and its finite element model.

The finite element method also has disadvantages. A computer, a reliable program, and intelligent use are essential. A general-purpose program has extensive documentation, which cannot be ignored. Experience and good engineering judgment are needed to define a good model. Many input data are required and voluminous output must be stored and understood. [22]

An iterative solution technique for a FEM solver was employed to solve the set of

equations sequentially and separately for each active degree of freedom. This approach is referred to as a segregated solver. This method is used because it substantially reduces the memory requirement compared to the other solvers used, such as the fully coupled method. Another major reason is FIDAP provide the means-VOF (Volume of Fluid) to model transient flows involving free surfaces of arbitrary shape. The capabilities constitute a powerful tool in simulating complex free surface deformations including folding and breakup.

FIDAP was used to solve the fluid and heat flow inside the molds. A "mapped" type mesh was used to discretize the geometry. The general purpose pre-processor GAMBIT^{TM} was used for the mesh generation.

A mapped mesh is a regular "checkerboard" mesh for surface areas that are typically used for more regular geometries. The complete finite element mesh for the heat transfer problem was constructed from a collection of mapped mesh areas. This technique is not automatic, as the geometry must be decomposed into regions that are suited to a mapped mesh.

A backward Euler (implicit) scheme was used to solve the three transient equations. Segregated iterative method was used to obtain the solution at each time step using fixed time step. Although one can generally obtain high order accuracy, when convection is strong compared to the diffusion and sharp gradients of the flow variables are encountered in the computational grid, unstable results are likely to occur. Streamline upwinding is used to stabilize the oscillations in the computations. This procedure can be applied globally or selectively to any or all primary flow variables that are governed by partial differential conservation equations. Mixed and discontinuous pressure

discretization approach are used, which means the pressure variable is discretized and contributes an additional degree of freedom to the system of unknowns to be solved; the pressure approximation is discontinuous across element boundaries

There are two general approaches that could be used to model the flow of the molten material into the melt. The first is to move the mesh with the melt. This approach requires the mesh to be continually recalculated and it requires a technique to couple the heat transfer to the solid. The second choice is to have the fluid move through a fixed mesh. This latter technique is the approach FIDAP uses and it will briefly be discussed here.

Free boundaries are considered to be surfaces on which discontinuities exist in one or more variables. Examples are free surfaces of fluids (open channel flow), material interfaces, shock waves, or interface between a fluid and deformable structures. Three types of problems arise in the numerical treatment of free boundaries: (1) their discrete representation, (2) their evolution in time, and (3) the manner in which boundary conditions are imposed on them. The process of embedding a discontinuous surface in a matrix of computational cells involves three separate tasks. First, it is necessary to devise a means of numerically describing the location and shape of the boundary. Second, an algorithm must be given for computing the time evolution of the boundary. Finally, a scheme must be provided for imposing the desired surface boundary conditions on the surrounding computational mesh. [23]

FIDAP refers to their implementation as the Volume of Fluid (VOF) method to simulate the free surface flows. [24] This tool is a filling process, which allows the simulation of complex free surface flows with an arbitrary shape in any situation including folding or break-up. The filling process is computed as follows:

- A Galerkin finite element method is used to resolve Navier-Stokes equations.
- Free surfaces are characterized by a Volume of Fluid type representation on the mesh, advection of the fluid is followed by a volume tracking method.
- On the basis of a given velocity field, a new fluid boundary is determined with the volume method. When the new fluid boundary is obtained, the Reynolds Average Navier-Stokes equations are solved using a finite element method. These two methods are thus applied in alternating deformations and decoupled in order to predict transient deformations.

A fraction F is defined whose value is unity at any point occupied by fluid and zero otherwise. The average value of F in a cell would then represent the fractional volume of the cell occupied by fluid. In particular, a unit value of F would correspond to a cell full of fluid, while a zero value would indicate that the cell contained no fluid. Cells with F values between zero and one must then contain a free surface. VOF method only requires one storage word for each mesh cell, which is consistent with the storage requirements for all other dependent variables.

Figure 3.4 a and b describe the schematic of a single fluid and two-fluid scenario. Figure 3.4 (a) is a single fluid scenario where both fluid and void contact a solid region. A melt-mold interfacial heat transfer coefficient is specified along the interface of the solid and fluid regions. The value of the coefficient is a specified value and is automatically defined to zero between the void and the solid (mold), because there is no heat transfer to the void region. Figure 3.4 (b) shows a two-fluid scenario. Two different heat transfer coefficients are used. One of them represents the full elements that define

the interface between fluid A and the solid. The other one relates to the empty elements that define the interface between B and the solid.

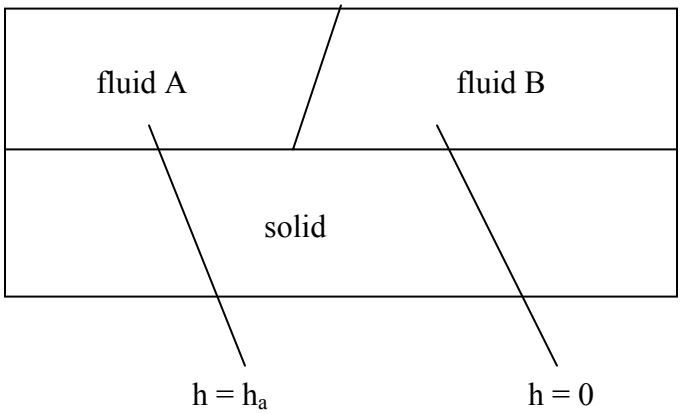

Figure 3.5 (a) Applied heat transfer coefficient for a single fluid scenario

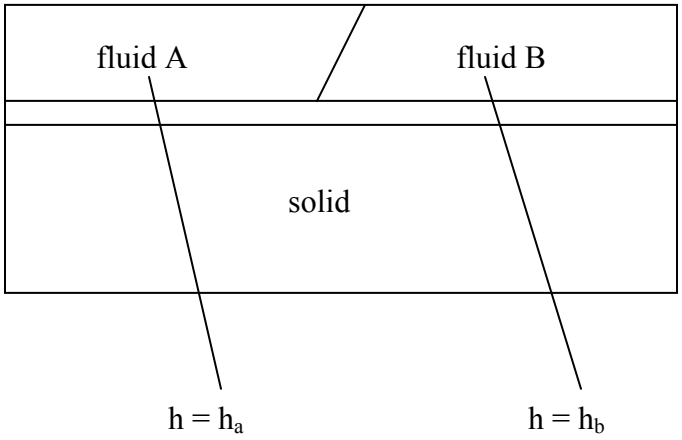

Figure 3.5 (b) Applied heat transfer coefficient for a two-fluid scenario

Here, an indicator function F is used to represent the fluid volume, which moves with the fluid. So the advection is governed by this function:

$$\frac{\partial F}{\partial t} + \overline{V} \cdot \nabla F = 0 \qquad (6)$$

The sharp interfaces are maintained by ensuring a sharp gradient of F. The value of this function is 1 when the cell of the meshing volume is filled and is equal to 0 when this cell is emptied. A steep gradient of F represents a free surface location.

$$F\ (\vec{x}\ ,\ t\ )\ =\ \begin{cases} 1\ Fluid \\ 0\ Void \end{cases} \tag{7}$$

The function F can be discretized as follows:

$$f_i\ =\ \tfrac{1}{V_i}\int FdV_{\ i} \quad \text{for element I} \tag{8}$$

The limits of integration are restricted to the volume of an element V_i. The value of f_i corresponds to a filled state, an emptied state, or fractional filled state. Thus f_i varies between 0 and 1. An element whose $f_i = 1$ is referred to as a filled element. An emptied element is denoted by $f_i = 0$. The value of f_i between 0 and 1 means a fractional fill or a free surface. [24][25]

The VOF method offers a region-following scheme with smaller storage requirements. Furthermore, because it follows regions rather than surface, all logic problems associated with intersecting surfaces are avoided with the VOF technique. The method is also applicable to three-dimensional computations, where its conservative use of stored information is highly advantageous. In principle, the method can be used to track surfaces of discontinuity in materials properties, in tangential velocity, or any other property. The particular case being represented determines the specific situations that must be applied at the location of the boundary. For situations where the surface does not remain fixed in the fluid, but has some additional relative motion, the equation of motion must be modified. Examples of such applications are shock waves, chemical reaction fronts, and boundaries between single-phase and two-phase fluid regions. [23]

3.3 Parametric Study

In order to test the impact of process parameters (temperature, pressure, alloying elements, etc.) on the casting process, a parametric study of the casting model was performed on different parameters to determine which process parameters are critical in manufacturing a suitable metallic fuel pin. For some specific properties, which are not available, it will parametrically vary these properties over the expected range to see how these properties might exhibit and determine how critical these properties are to the processing of the fuel.

Parameter study efforts centered around model development and the analysis of the impact of mold preheating on heat transfer into the mold. Inner radius is already set by the Argonne National Laboratory.

Normally, the way the heat flows across the metal and mold surfaces directly affects the evolution of solidification, and plays a notable role in determining the freezing conditions within the metal. When metal and mold surfaces are brought into contact an imperfect junction is formed. While uniform temperature gradients can exist in both metal and mold, the junction between the two surfaces creates a temperature drop, which is dependent upon the thermophysical properties of the contacting materials, the casting and mold geometry, the roughness of mold contacting surface, the presence of the gaseous and non-gaseous interstitial media, the melt superheat, contact pressure and initial temperature of the mold. Because the two surfaces in contact are not perfectly flat, when the interfacial contact pressure is reasonably high, most of the energy passed through a limited number of actual contact spots. [26] The heat flow across the casting-

mold interface can be characterized by a macroscopic average metal-mold interfacial heat transfer coefficient (h_i), given by

$$h_i = \frac{q}{A(T_{1C} - T_{1M})} \tag{9}$$

The heat transfer coefficient shows a high value in the initial stage of solidification, the result of good surface conformity between the liquid core and the solidified shell. As the solidification progresses the mold expands due to the absorption of heat and the solid metal shrinks during cooling and as a result a gap develops because pressure becomes insufficient to maintain a conforming contact at the interface. Once the air gaps form, the heat transfer across the interface decreases rapidly and a relatively constant value of h_i is attained. The ways of heat transfer here are assumed to be due to both conduction through isolated metal-mold contacts and through gases present in the gap and radiation between the surfaces. [26]

Previous research shows that the process of thermal energy stored in liquid metal to the mold at the metal-mold interface during solidification is determined by the heat transfer coefficient at the interface. The quality of the final product-fuel pin is directly affected by the interfacial heat transfer conditions, which is mostly from heat transfer coefficient.

Average fill velocity was also changed to see how do they affect the filling process.

Tables through 3.1 and Table 3.2 show all the parameter values used under various simulation circumstance.

Table 3.3 and 3.4 show all basic physical properties of mold and melt respectively.

Table 3.1 Parameters selected for copper simulation

	Mold length = 0.5 m		
	HT Coefficient = 2000,5000 W/m^{2}K		
Copper Mold	Mold Preheating Temperature (^{o}C)		
Inlet Velocity (m/s)	400	800	1200
0.1	×	×	×
1.0	×	×	×
2.0	×	×	×

Table 3.2 Parameters selected for quartz simulation

	Mold length = 0.5 m		
	HT Coefficient = 2000, 5000 W/m^{2}K		
Quartz Mold	Mold Preheating Temperature (^{o}C)		
Inlet Velocity (m/s)	400	800	1200
0.1	×	×	×
1.0	×	×	×
2.0	×	×	×

Table 3.3 Physical properties of mold materials

Physical Properties of Mold Materials	"Copper"	Quartz
Thermal Conductivity (W/m·^{o}C)	320	1.4
Specific Heat (J/Kg·^{o}C)	380	670
Density (Kg/ m^3)	8933	2200

Table 3.4 Physical properties of melt

Melt Contents	Pu, Zr, Am, etc
Thermal Conductivity (W/m·K)	6
Specific Heat (J/Kg·^{o}C)	150
Density (Kg/ m^3)	19800
Viscosity (N·s/ m^2)	0.1

CHAPTER 4

RESULTS AND DISCUSSION

The parametric study centered on the model development and the analysis of the impact of the possible parameters on the heat transfer into the mold. The way the heat flows across the metal-mold surfaces directly affects the evolution of solidification, and plays a notable role in determining the freezing conditions within the melt.

During the simulation, the filling velocity is changed from 0.1 m/s to 1.0 m/s to 2.0 m/s to see how the filling velocity affects the heat into the mold. Mold preheating temperature will also be changed from 400 ^{o}C to 800 ^{o}C and 1200 ^{o}C to show their effects. Two different heat transfer coefficients were selected to simulate to see how this factor affects the heat transferring into molds. Copper and quartz were used to see how different mold materials control the heat transfer.

4.1 Temperature Profile for Copper Molds

4.1.1 Temperature Profile With Heat Transfer Coefficient 2000 W/m^{2}K And Initial Filling Velocity 0.1 m/s

- The conditions for each model included:
- Melt temperature of 1500 ^{o}C.
- Average fill velocity of 0.1 m/s
- Mold thermal properties assumed to be similar to copper

- Pin diameter of 0.008 m**,** Mold outside diameter of 0.016 m
- Mold length of 0.50 m
- Properties of melt assumed to be dependent on plutonium, americium, and zirconium
- Heat transfer coefficient between the melt and the mold assumed to be 2,000 W/m^2K, unless otherwise noted
- Initial mold temperatures were varied (1200 ^oC, 800 ^oC, or 400 ^oC)

Figures 4.1 through 4.3 below show radial temperature profiles of the melt just behind the melt front as it advances into the mold. This region would be the melt region that would solidify most rapidly. From the plots, a big temperature drop can be found when the melt reaches the mold surfaces. There is high temperature difference between the melt and mold inner surface. The temperature drop near the mold surface increases using lower mold temperature.

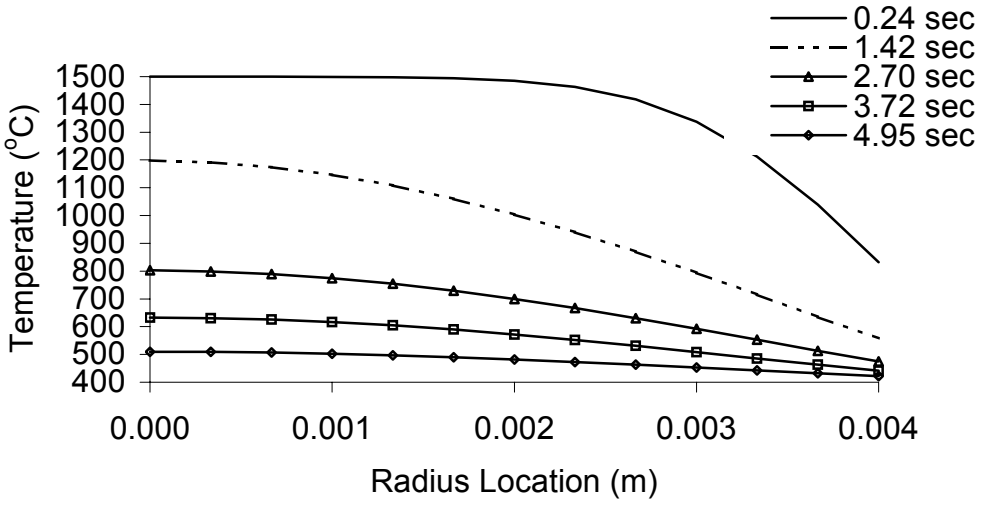

Figure 4.1 Temperature profiles form the centerline projected radially outward for an initial mold temperature of 400 ^oC. h = 2000 W/m^2K, $V_{filling}$ = 0.1 m/s.

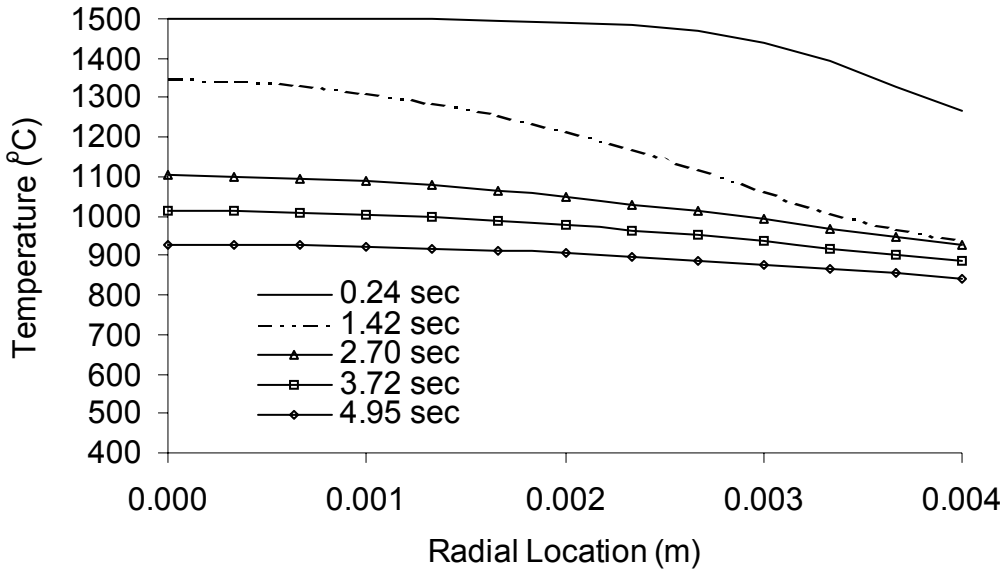

Figure 4.2 Temperature profiles form the centerline projected radially outward for an initial mold temperature of 800 ^{o}C. h = 2000 W/m^{2}K, $V_{filling}$ = 0.1m/s.

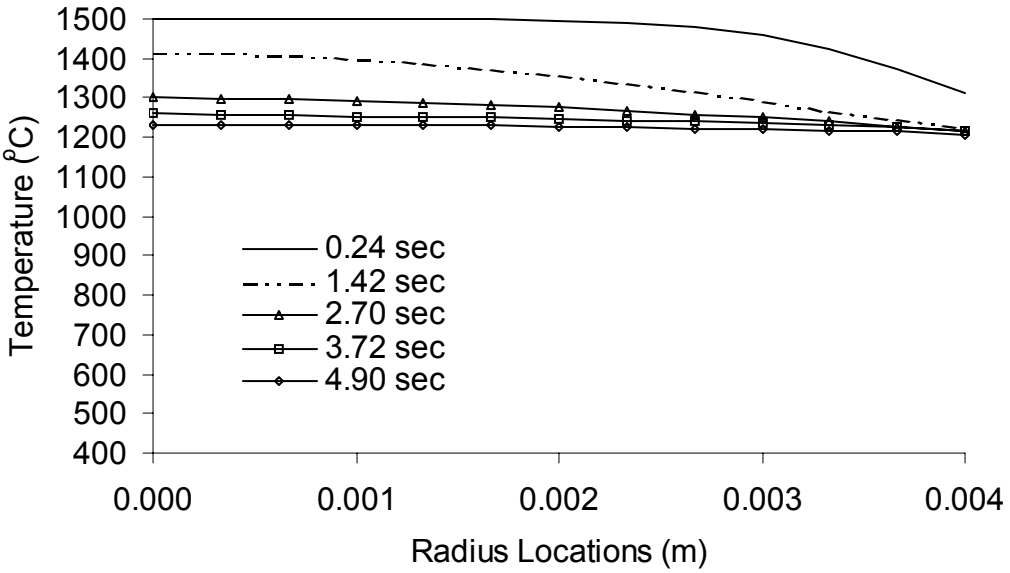

Figure 4.3 Temperature profiles form the centerline projected radially outward for an initial mold temperature of 1200 ^{o}C. h = 2000 W/m^{2}K, $V_{filling}$ = 0.1m/s.

Figure 4.4 and Figure 4.5 show the mold preheating effect on the heat transfer from melt into the mold. Figure 4.4 shows the temperature profile at 1.42 second in the radial

direction during different preheating temperature condition. Higher preheating temperature will prevent the heat transferring into mold, which means it will take more time to reach the same location. Figure 4.5 shows the radial temperature profile at 3.72 second during different mold preheating temperature.

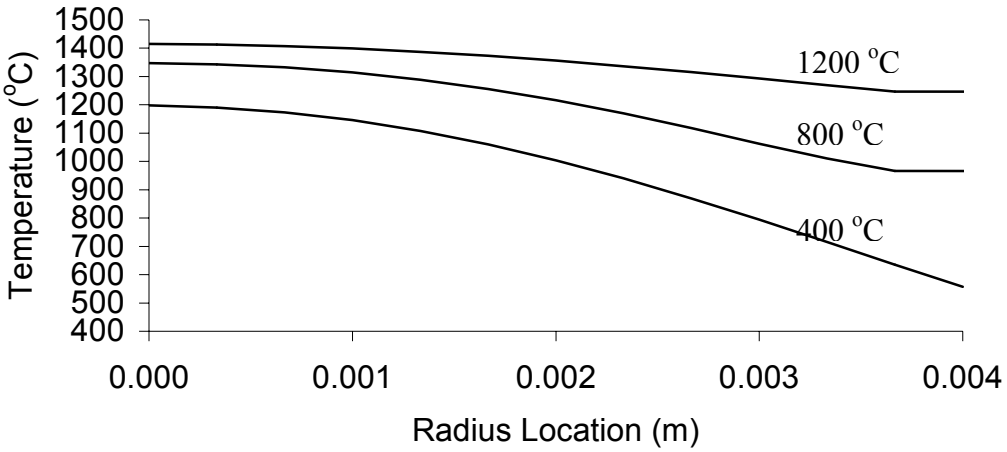

Figure 4.4 Temperature profiles from the centerline projected radially outward at 1.42 seconds. Lower to upper curves represent mold temperature of 400 °C, 800 °C and 1200 °C. h = 2000 W/m^{2}K, $V_{filling}$ = 0.1 m/s

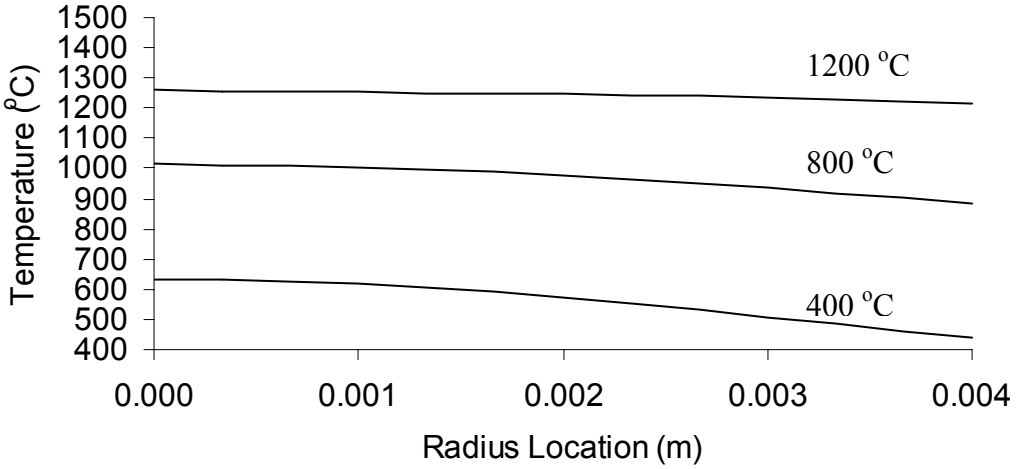

Figure 4.5 Temperature profiles from the centerline projected radially outward at 3.72 seconds. Lower to upper curves represent mold temperature of 400 °C, 800 °C and 1200 °C. h = 2000 W/m^{2}K, $V_{filling}$ = 0.1 m/s

Figures 4.6 through 4.8 show temperature profiles of the melt along the mold-melt interface as the flow enters the mold. The small "bump" on each of the profiles is the direct result of the initial conditions (large temp change rate). To start the simulation, a small region of the mold is considered "filled" (0.020 m of the 0.500 m length). This fluid is at an initial condition of 1500^{o}C. The fluid has already filled a portion of the mold without undergoing any cooling due to the mold. This fluid does not undergo that initial rapid cooling that any subsequent fluid entering the computational domain experiences. This temperature result is not significantly "smeared out" as time advances because of the low thermal conductivity of the melt (6 W/mK). Effectively, one can ignore this portion of the curve when interpreting the numerical results.

The results show that the temperature will change slower if setting up higher preheating mold temperature. This can be explained that higher mold preheating temperature will decrease the temperature difference between mold inner surface and the melt, further decrease the heat transfer coefficient.

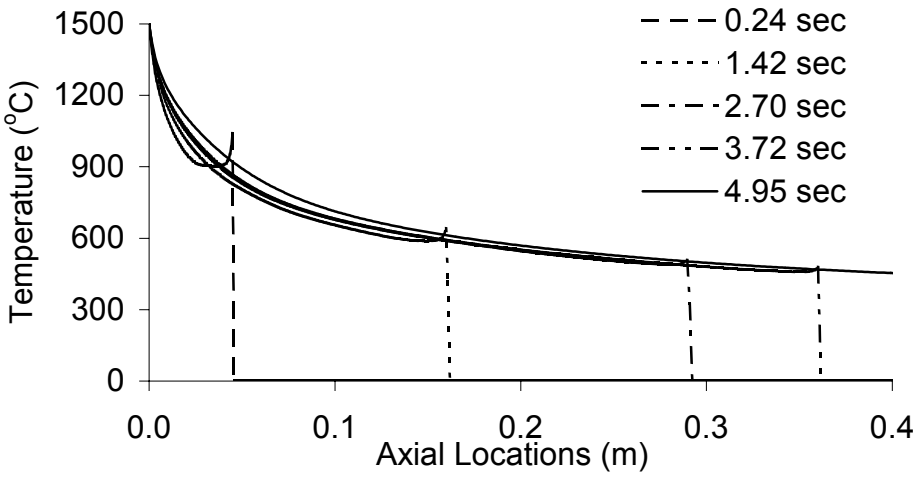

Figure 4.6 Temperature profiles of melt near the melt-mold interface as the flow enters the mold, an initial mold temperature 400 ^{o}C. h = 2000 W/m^{2}K, $V_{filling}$ = 0.1 m/s

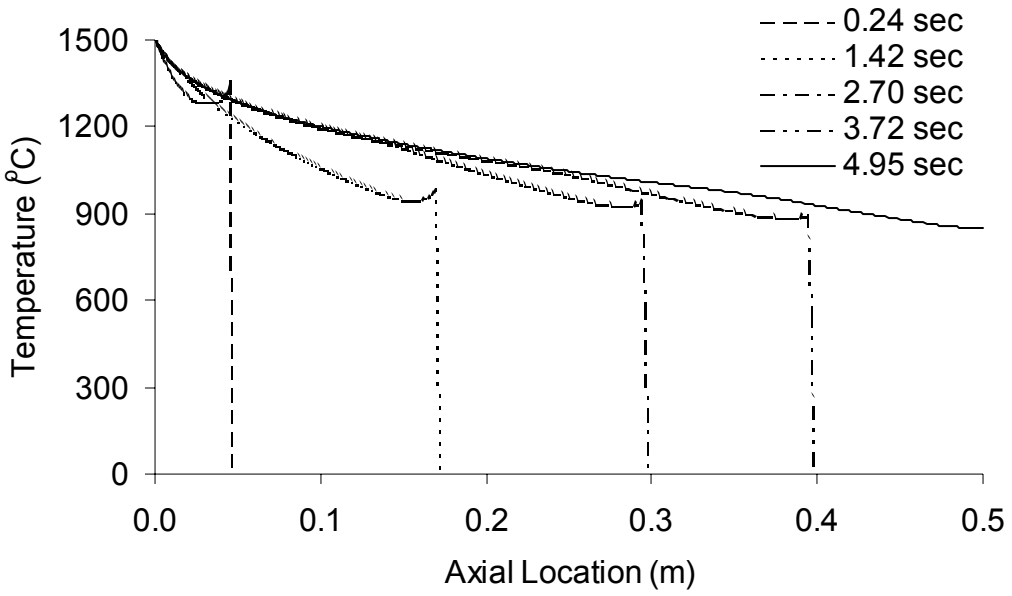

Figure 4.7 Temperature profiles of melt near the melt-mold interface as the flow enters the mold with an initial mold temperature 800 ^{o}C. h = 2000 W/m^{2}K, $V_{filling}$ = 0.1 m/s

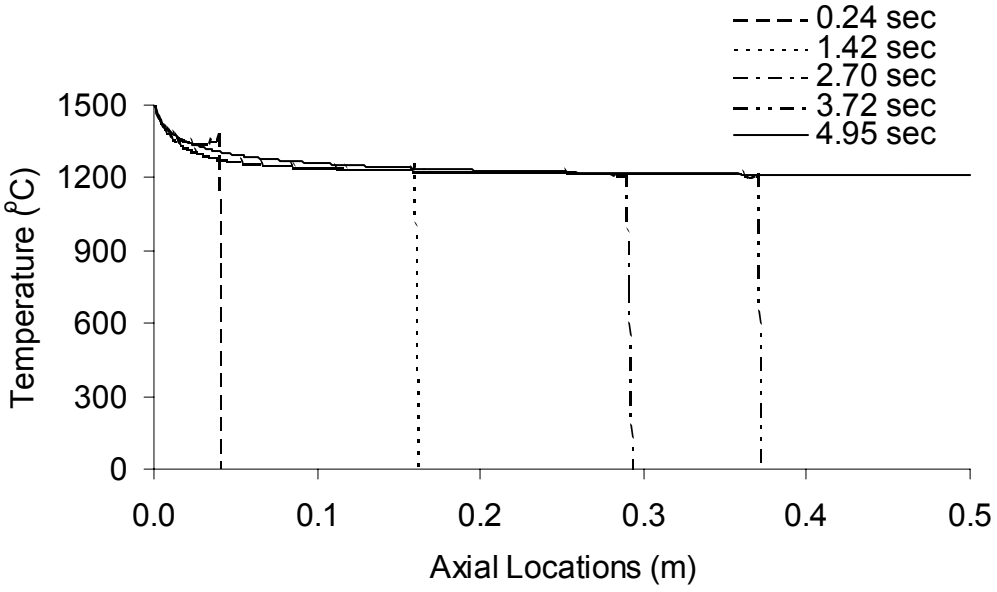

Figure 4.8 Temperature profiles of melt near the melt-mold interface as the flow enters the mold with an initial mold temperature 1200 ^{o}C. h = 2000 W/m^{2}K, $V_{filling}$ = 0.1 m/s

Temperature profiles along the melt-mold interface during different initial preheating mold preheating temperature of 400 ^{o}C, 800 ^{o}C and 1200 ^{o}C are shown in Figures 4.9 &

4.10. As observed from the plots, the mold preheating temperature greatly impacts the cooling rate of the melt as it flows into the mold.

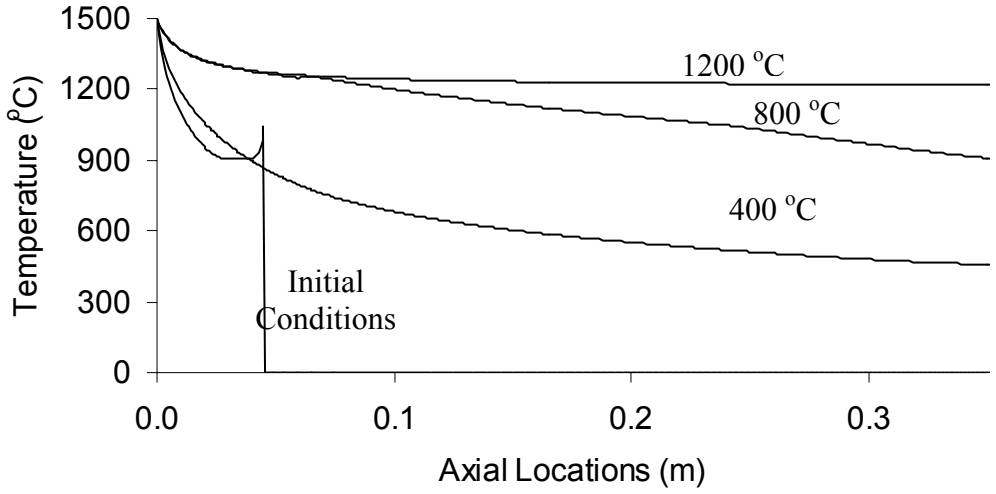

Figure 4.9 Temperature profiles of melt material near the melt-mold interface at 3.72 second. Lower to upper curves represent mold temperature of 400 °C, 800 °C and 1200 °C. h = 2000 W/m^{2}K, $V_{filling}$ = 0.1 m/s

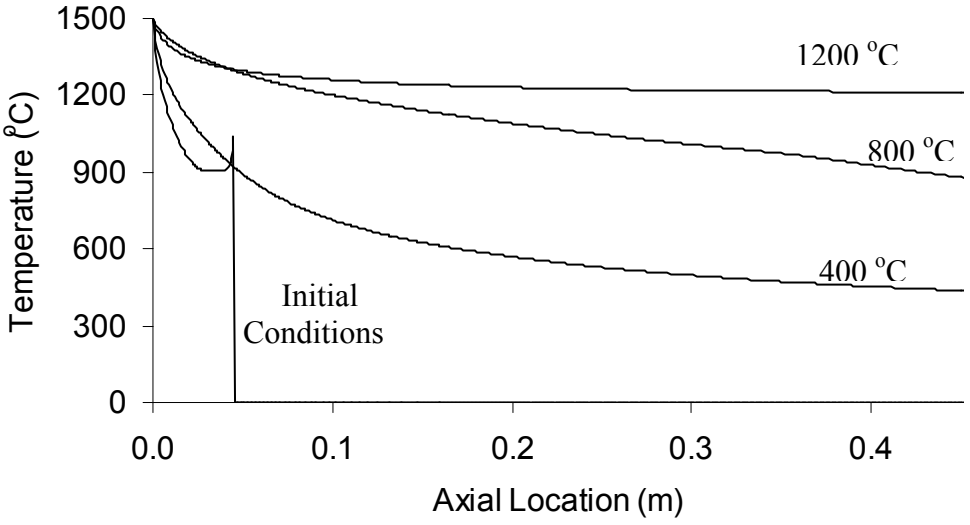

Figure 4.10 Temperature profiles of melt material near the melt-mold interface at 4.95 second. Lower to upper curves represent mold temperature of 400 °C, 800 °C and 1200 °C. h = 2000 W/m^{2}K, $V_{filling}$ = 0.1 m/s

4.1.2 Temperature Profile With Heat Transfer Coefficient 2000 W/m^2K And Initial Filling Velocity 1.0 m/s

- The conditions for each model included:
- Melt temperature of 1500 ^oC.
- Average fill velocity of 1.0 m/s
- Mold thermal properties assumed to be similar to copper
- Pin diameter of 0.008 m
- Mold outside diameter of 0.016 m
- Mold length of 0.50 m
- Properties of melt assumed to be dependent on plutonium, americium, and zirconium
- Heat transfer coefficient between the melt and the mold assumed to be 2,000 W/m^2K, unless otherwise noted
- Initial mold temperatures were varied (1200 ^oC, 800 ^oC, or 400 ^oC)

Figures 4.11 through 4.13 below show radial temperature profiles of the melt just behind the melt front as it advances into the mold. This region would be the melt region that would solidify most rapidly. From the plots, a big temperature drop can be found when the melt reaches the mold surfaces. There is high temperature difference between the melt and mold inner surface. The temperature drop near the mold surface increases using lower mold temperature.

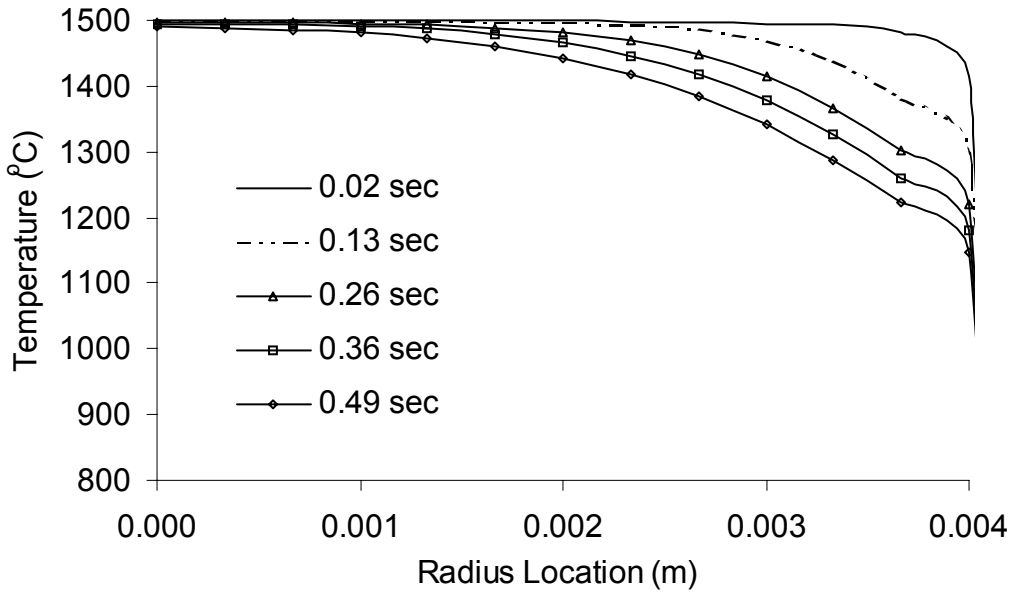

Figure 4.11 Temperature profiles form the centerline projected radially outward for an initial mold temperature of 400 ^{o}C. The axial location of each profile is slightly behind the front of the melt. h = 2000 W/m^{2}K, $V_{filling}$ = 1.0 m/s.

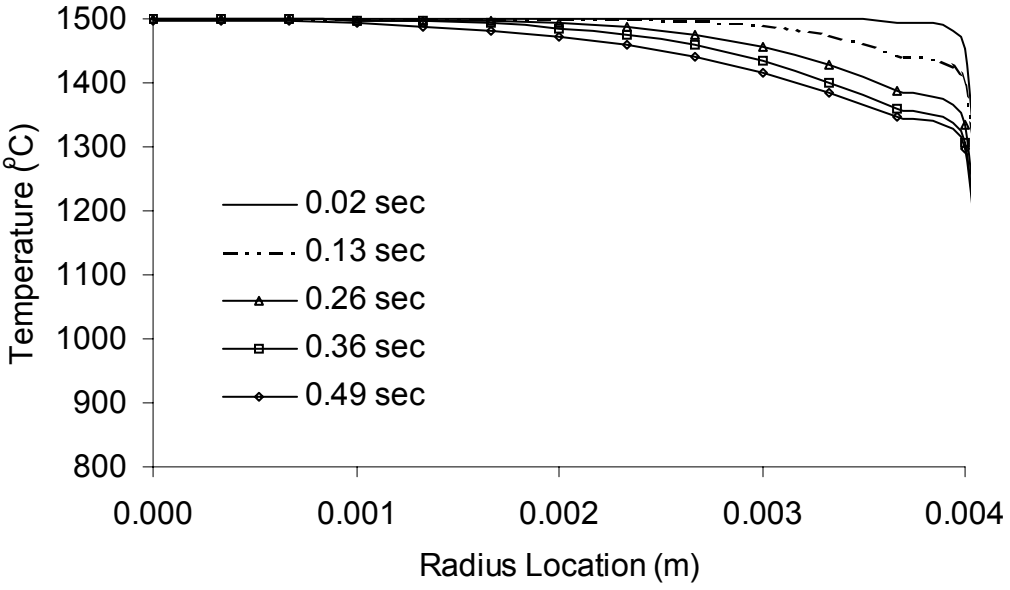

Figure 4.12 Temperature profiles form the centerline projected radially outward for an initial mold temperature of 800 ^{o}C. h = 2000 W/m^{2}K, $V_{filling}$ = 1.0 m/s.

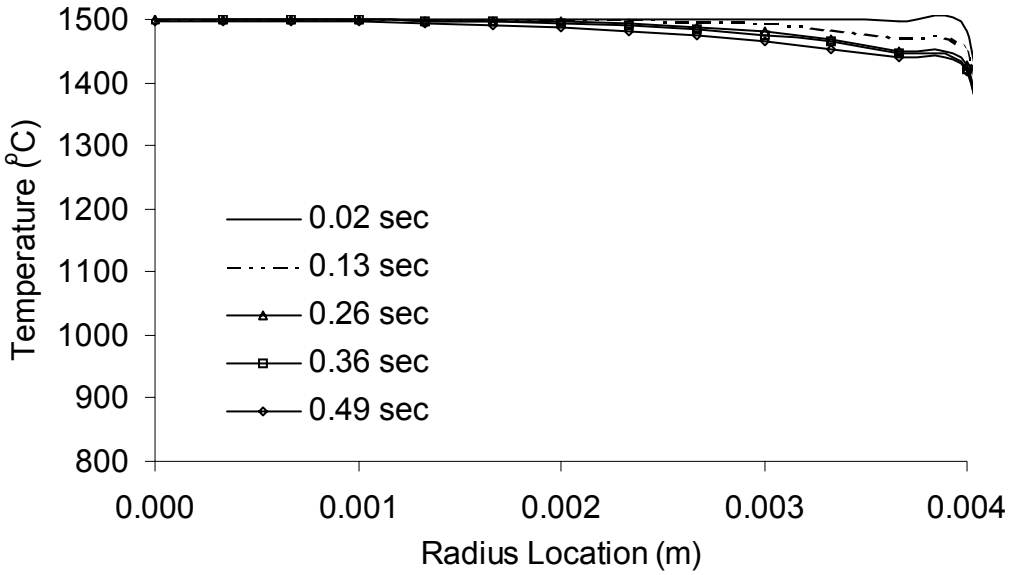

Figure 4.13 Temperature profiles form the centerline projected radially outward for an initial mold temperature of 1200 ^{o}C. h = 2000 W/m^{2}K, $V_{filling}$ = 1.0 m/s.

Figures 4.14 and 4.15 show the mold preheating effect on the heat transfer from melt into the mold. Figure 4.14 shows the temperature profile at 0.13 second in the radial direction during different preheating temperature condition. Higher preheating temperature will prevent the heat transferring into mold, which means it will take more time to reach the same location. Figure 4.15 shows the radial temperature profile at 0.36 second during different mold preheating temperature.

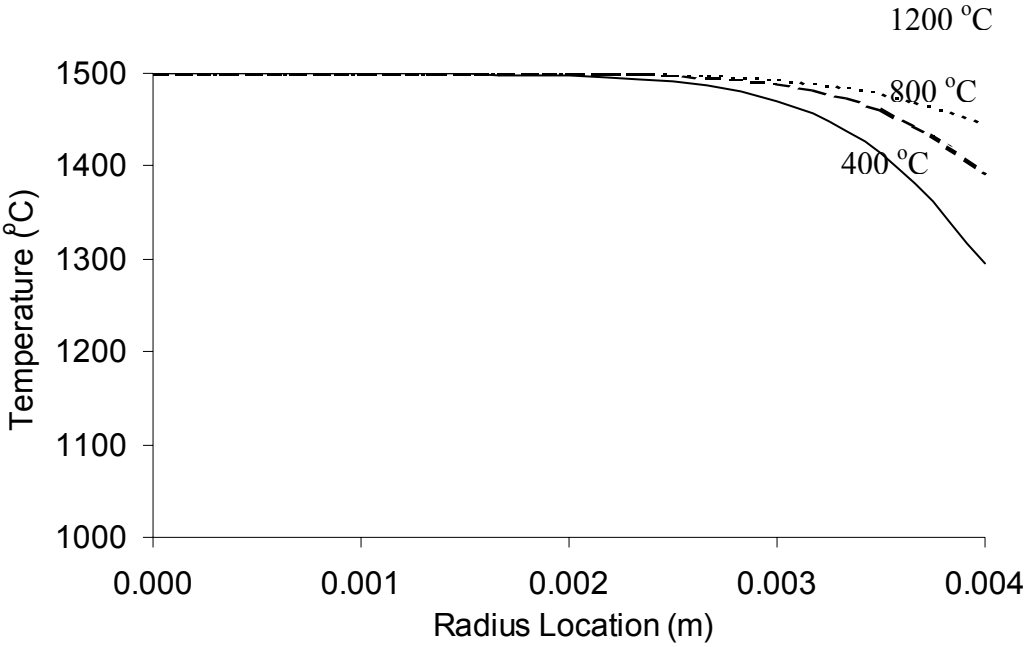

Figure 4.14 Temperature profiles from the centerline projected radially outward at 0.13 seconds. Lower to upper curves represent mold temperature of 400 °C, 800 °C and 1200 °C. h = 2000 W/m^{2}K, $V_{filling}$ = 1.0 m/s

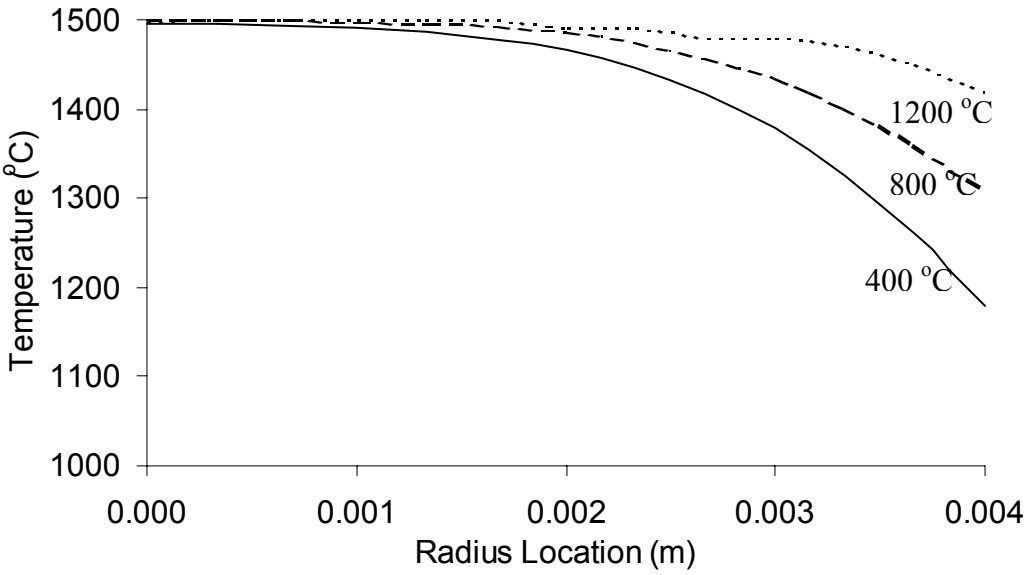

Figure 4.15 Temperature profiles from the centerline projected radially outward at 0.36 seconds. Lower to upper curves represent mold temperature of 400 °C, 800 °C and 1200 °C. h = 2000 W/m^{2}K, $V_{filling}$ = 1.0 m/s

Figures 4.16 through 4.18 show temperature profiles of the melt along the mold-melt interface as the flow enters the mold. The small "bump" on each of the profiles is the direct result of the initial conditions . To start the simulation, a small region of the mold is considered "filled" (0.020 m of the 0.500 m length). This fluid is at an initial condition of 1500^{o}C. The fluid has already filled a portion of the mold without undergoing any cooling due to the mold. This fluid does not undergo that initial rapid cooling that any subsequent fluid entering the computational domain experiences. This temperature result is not significantly "smeared out" as time advances because of the low thermal conductivity of the melt (6 W/mK). Effectively, one can ignore this portion of the curve when interpreting the numerical results.

The results show that the temperature will change slower if setting up higher preheating mold temperature. This can be explained that higher mold preheating temperature will decrease the temperature difference between mold inner surface and the melt, further decrease the heat transfer coefficient.

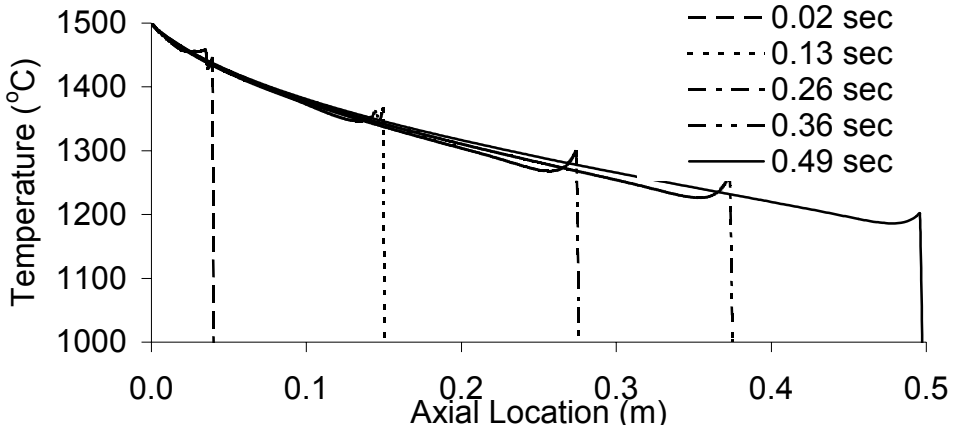

Figure 4.16 Temperature profiles of melt near the melt-mold interface as the flow enters the mold. An initial mold temperature 400 ^{o}C. h = 2000 W/m^{2}K, $V_{filling}$ = 1.0 m/s

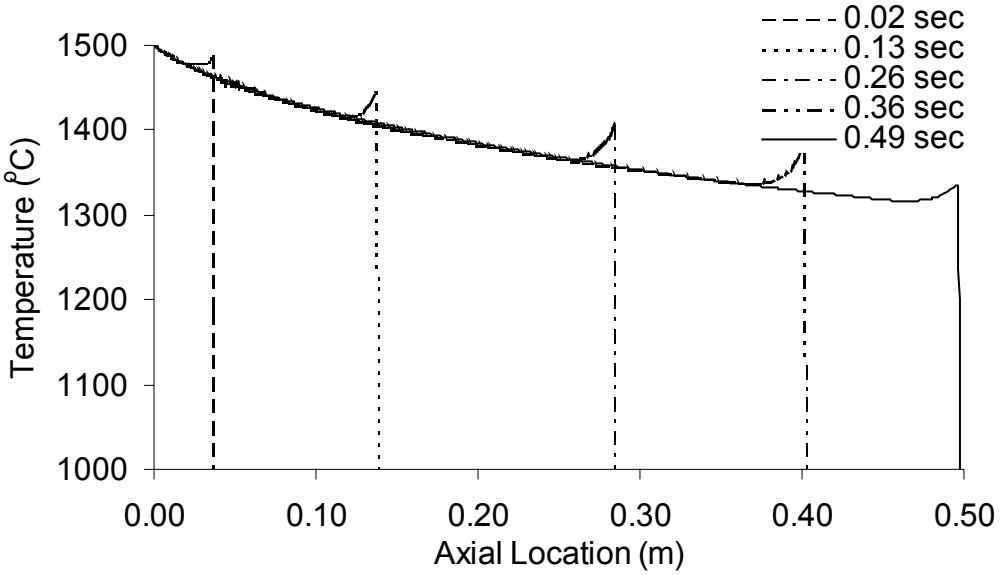

Figure 4.17 Temperature profiles of melt near the melt-mold interface as the flow enters the mold with an initial mold temperature 800 ^{o}C. h = 2000 W/m^{2}K, $V_{filling}$ = 1.0 m/s

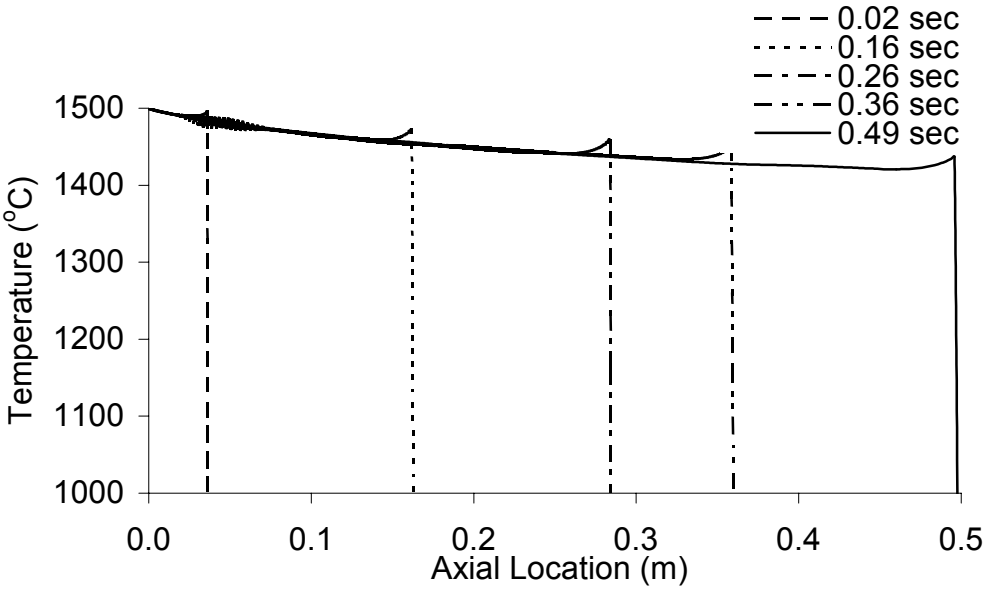

Figure 4.18 Temperature profiles of melt near the melt-mold interface as the flow enters the mold with an initial mold temperature 1200 ^{o}C. h = 2000 W/m^{2}K, $V_{filling}$ = 1.0 m/s

Temperature profiles along the melt-mold interface during different initial preheating mold preheating temperature of 400 ^{o}C, 800 ^{o}C and 1200 ^{o}C are shown in Figures 4.19 & 4.20. As observed from the plots, the mold preheating temperature greatly impacts the cooling rate of the melt as it flows into the mold.

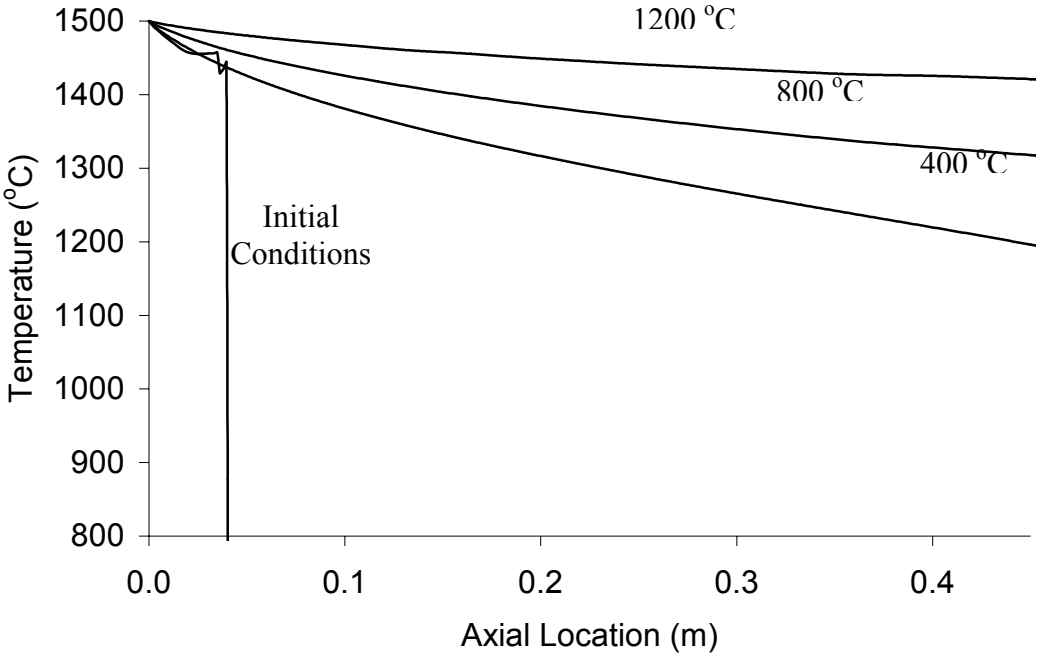

Figure 4.19 Temperature profiles of melt material near the melt-mold interface at 0.49 second. Lower to upper curves represent mold temperature of 400 ^{o}C, 800 ^{o}C and 1200 ^{o}C. h = 2000 W/m^{2}K, $V_{filling}$ = 1.0 m/s

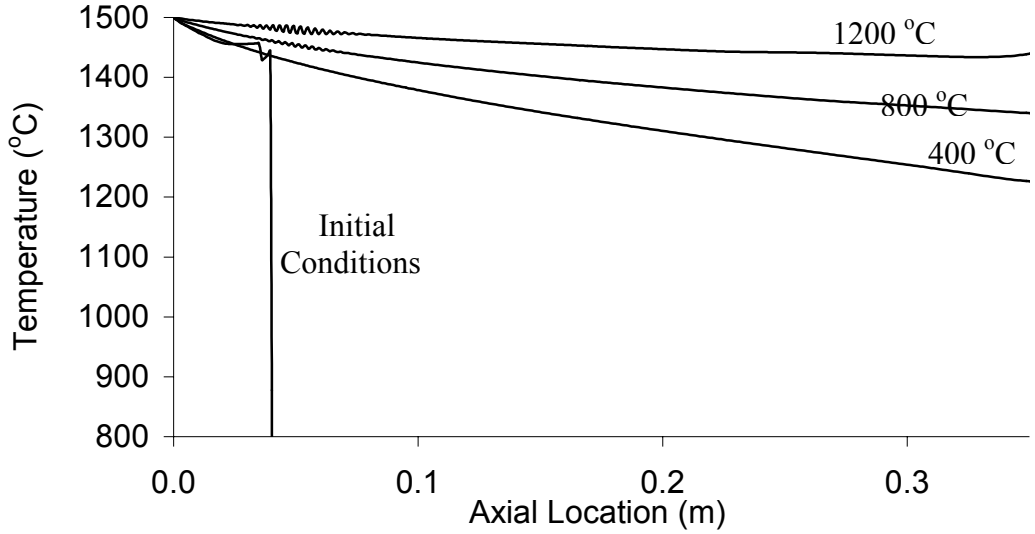

Figure 4.20 Temperature profiles of melt material near the melt-mold interface at 0.36 second. Lower to upper curves represent mold temperature of 400 °C, 800 °C and 1200 °C. h = 2000 W/m^{2}K, $V_{filling}$ = 1.0 m/s

4.1.3 Temperature Profile With Heat Transfer Coefficient 2000 W/m^{2}K And Initial Filling Velocity 2.0 m/s

The conditions for each model included:

- Melt temperature of 1500 °C.
- Average fill velocity of 2.0 m/s
- Mold thermal properties assumed to be similar to copper
- Pin diameter of 0.008 m
- Mold outside diameter of 0.016 m
- Mold length of 0.50 m
- Properties of melt assumed to be dependent on plutonium, americium, and zirconium

- Heat transfer coefficient between the melt and the mold assumed to be 2,000 W/m^2K, unless otherwise noted
- Initial mold temperatures were varied (1200 ^oC, 800 ^oC, or 400 ^oC)

Figures 4.21 through 4.23 show radial temperature profiles of the melt just behind the melt front as it advanced into the mold. Compared with Figures 4.1 through 4.3, and figure 4.11, 4.13 we can see the difference due to the effect of increased initial velocity (from 0.1 m/s to 1.0 m/s to 2.0 m/s). The heat transfer into mold with higher filling velocity is faster than lower initial velocity. From the plots a big temperature drop can be found when the melt reaches the mold surface. There is high temperature difference between the melt and mold inner surface, and this one depends on the preheating.

Figures 4.24 through 4.26 show the temperature profile of the melt along the melt-mold interface as the flow enters the mold. The temperature along the interface will changes more slowly if set up higher mold preheating temperature. This can be explained because the high mold preheating temperature decrease the temperature difference between the interface, further decrease the metal-mold interfacial heat transfer coefficient.

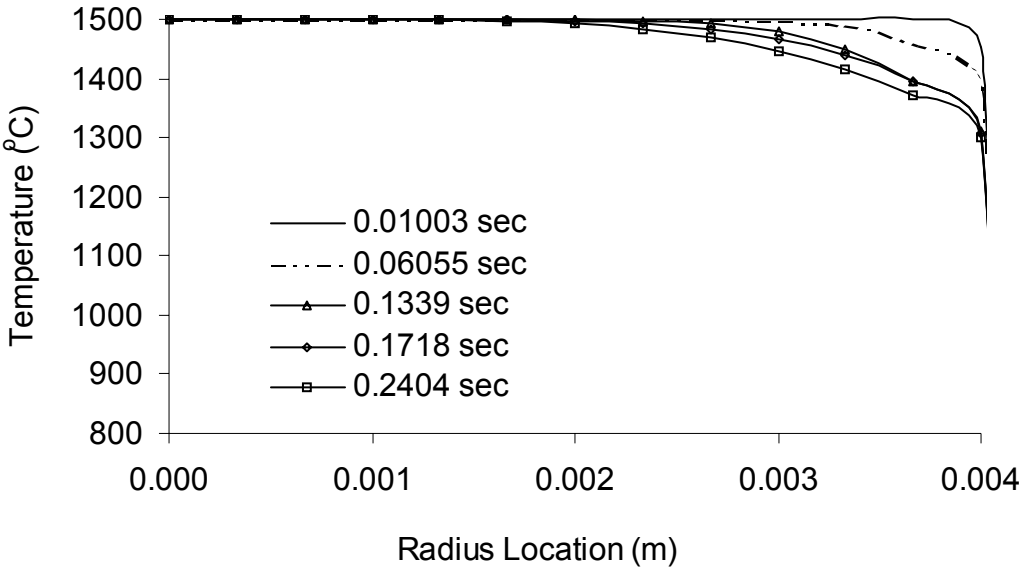

Figure 4.21 Temperature profiles form the centerline projected radially outward for an initial mold temperature of 400 ^{o}C. h = 2000 W/m^{2}K, $V_{filling}$ = 2.0 m/s.

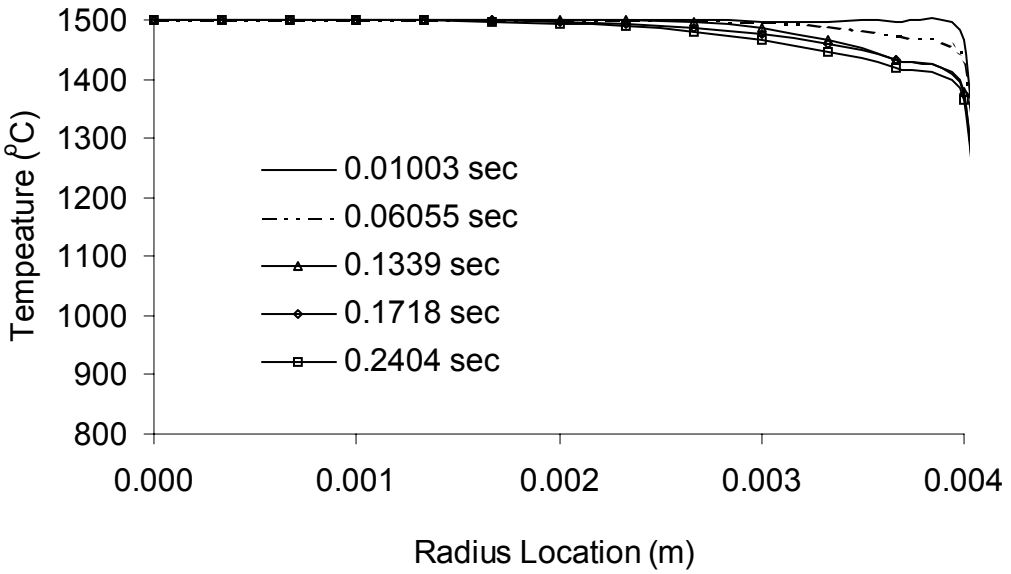

Figure 4.22 Temperature profiles form the centerline projected radially outward for an initial mold temperature of 800 ^{o}C. h = 2000 W/m^{2}K, $V_{filling}$ = 2.0 m/s.

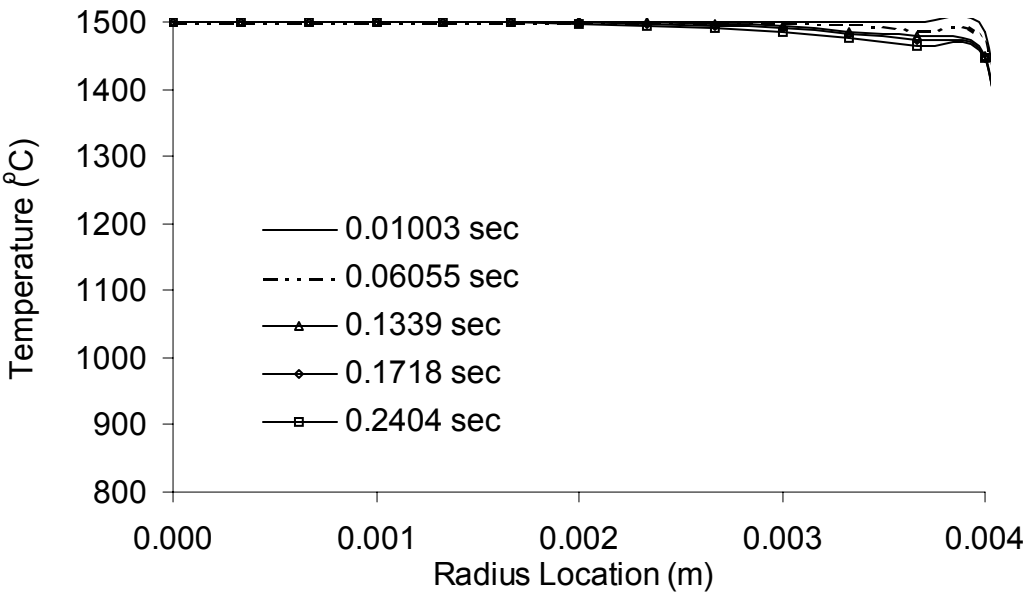

Figure 4.23 Temperature profiles form the centerline projected radially outward for an initial mold temperature of 1200 ^{o}C.
h = 2000 W/m^{2}K, $V_{filling}$ = 2.0 m/s.

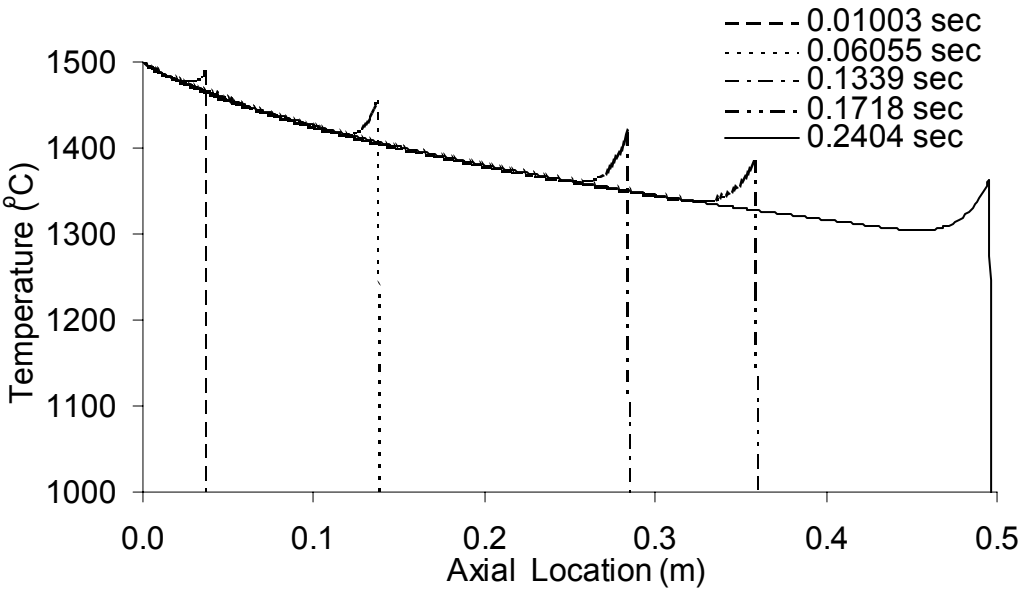

Figure 4.24 Temperature profiles of melt near the melt-mold interface as the flow enters the mold with an initial mold temperature 400 ^{o}C.
h = 2000 W/m^{2}K, $V_{filling}$ = 2.0 m/s.

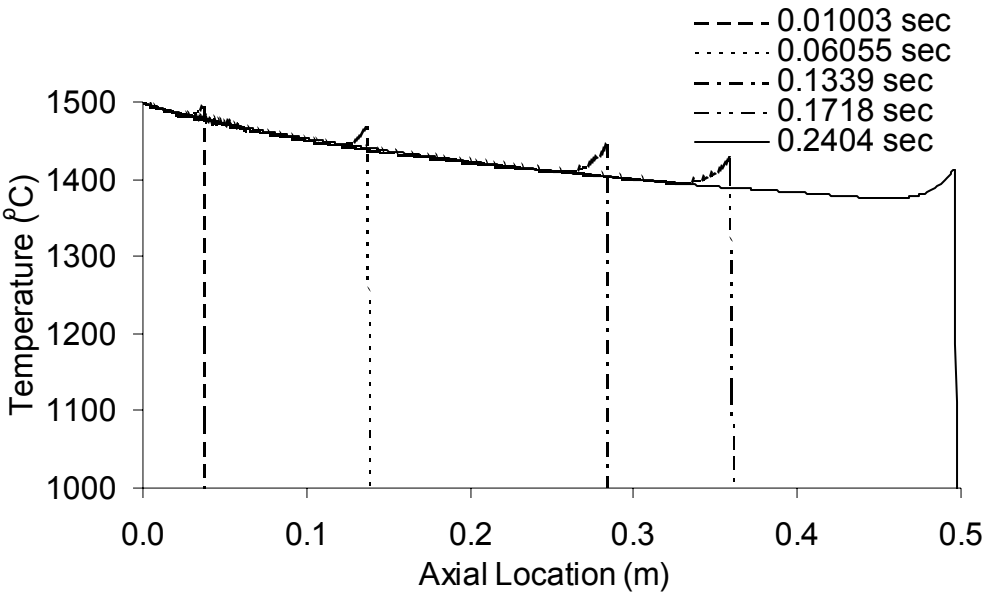

Figure 4.25 Temperature profiles of melt near the melt-mold interface as the flow enters the mold with an initial mold temperature 800 ^{o}C.
h = 2000 W/m^{2}K, $V_{filling}$ = 2.0 m/s.

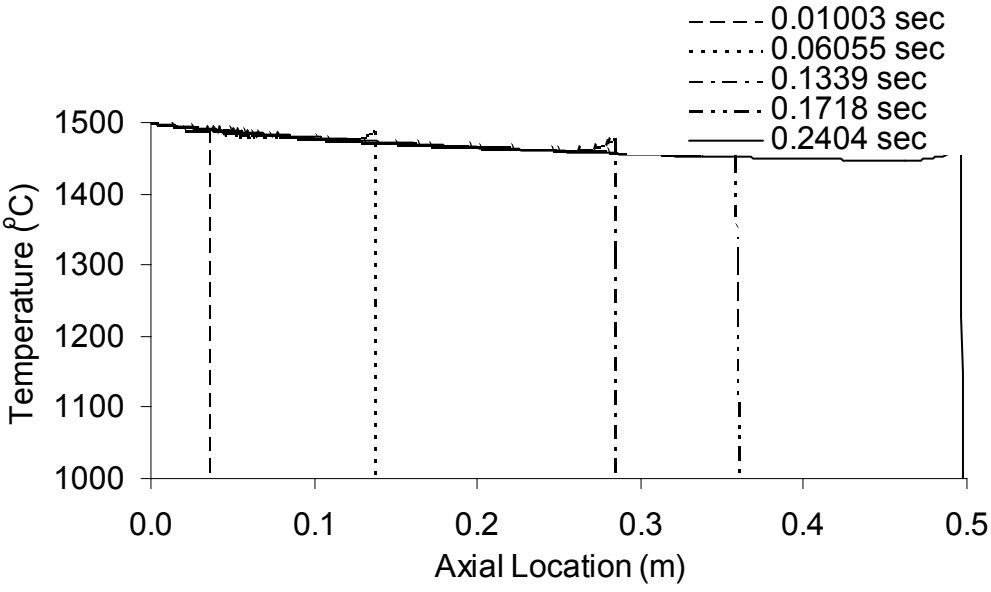

Figure 4.26 Temperature profiles of melt near the melt-mold interface as the flow enters the mold with an initial mold temperature 1200 ^{o}C.
h = 2000 W/m^{2}K, $V_{filling}$ = 2.0 m/s.

Figures 4.27 and 4.28 show the mold preheating effect on the heat transfer from the melt into the mold. Figure 4.27 shows the temperature profiles at 0.06 second in the radial direction during different preheating temperature condition. The heat transferring into mold will be slower if using higher preheating temperature. Figure 4.28 shows the radial temperature profile at 0.18 second during different mold preheating temperature.

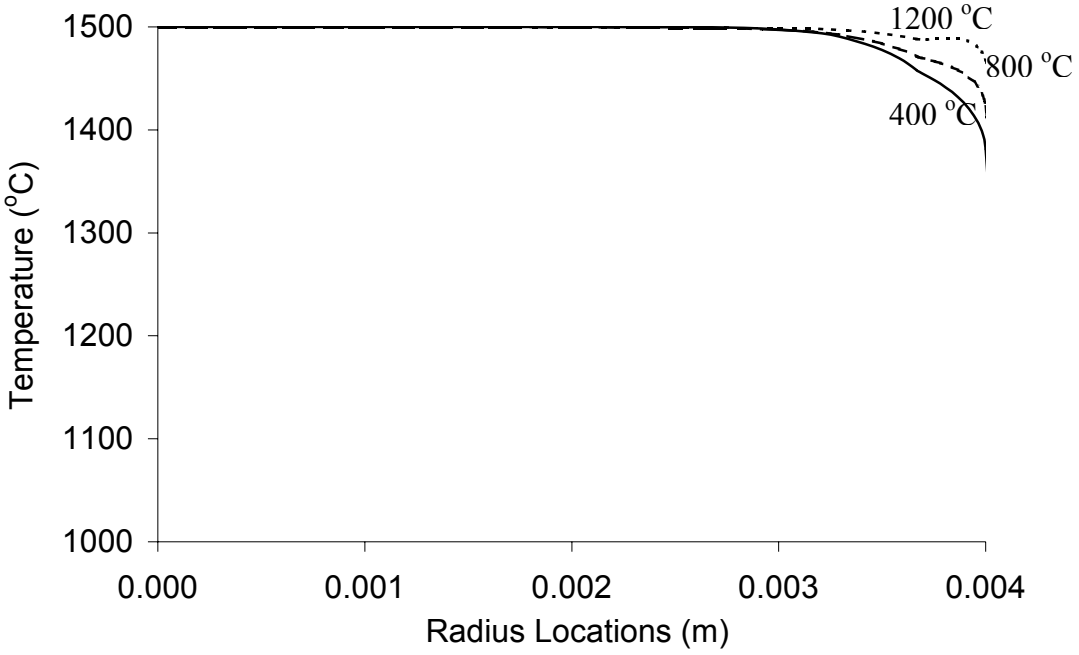

Figure 4.27 Temperature profiles from the centerline projected radially outward for copper mold 0.06 second. Lower to upper curves represent mold temperature of 400 °C, 800 °C and 1200 °C. h = 2000 W/m^{2}K, $V_{filling}$ = 2.0 m/s.

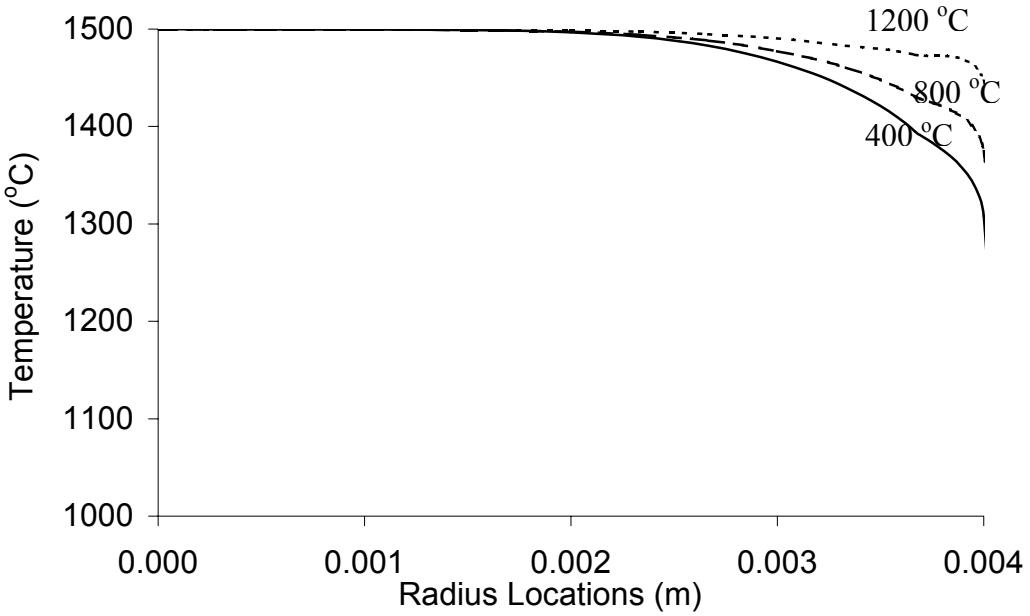

Figure 4.28 Temperature profiles from the centerline projected radially outward for copper mold 0.18 second. Lower to upper curves represent mold temperature of 400 °C, 800 °C and 1200 °C. h = 2000 W/m^{2}K, $V_{filling}$ = 2.0 m/s.

Figures 4.29 shows the temperature profiles along the melt-mold interface during different initial preheating mold temperature 400 °C, 800 °C and 1200 °C. There are more wiggles near the filling entrance when the preheating temperature is higher. These wiggles indicate that the heat transfer will be slower if the preheating mold temperature is higher. The cooling of the melt using 2.0 m/s is faster than using 1.0m/s, as compared with Figure 4.20.

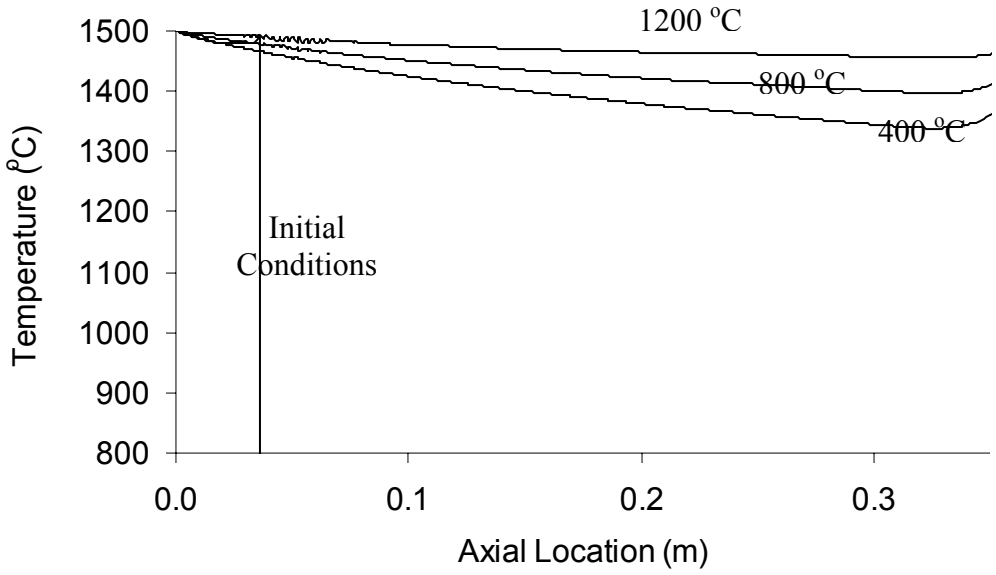

Figure 4.29 Temperature profiles of melt material near the melt-mold interface at 0.18 second. Lower to upper curves represent mold temperature of 400 °C, 800 °C and 1200 °C. h = 2000 W/m^{2}K, $V_{filling}$ = 2.0 m/s.

4.1.4 Impact Of The Initial Velocity On The Cooling Of The Melt

Figures 4.30 through 4.32 how the temperature profiles of the melt materials near the melt-mold interface with initial filling velocity 0.1 m/s, 1.0 m/s and 2.0 m/s. The temperature distribution shows that higher filling velocity increases the heat transfer into the molds. The wiggles can also be explained from a velocity point. Lower filling velocity causes the heat transfer to become slower in a short time.

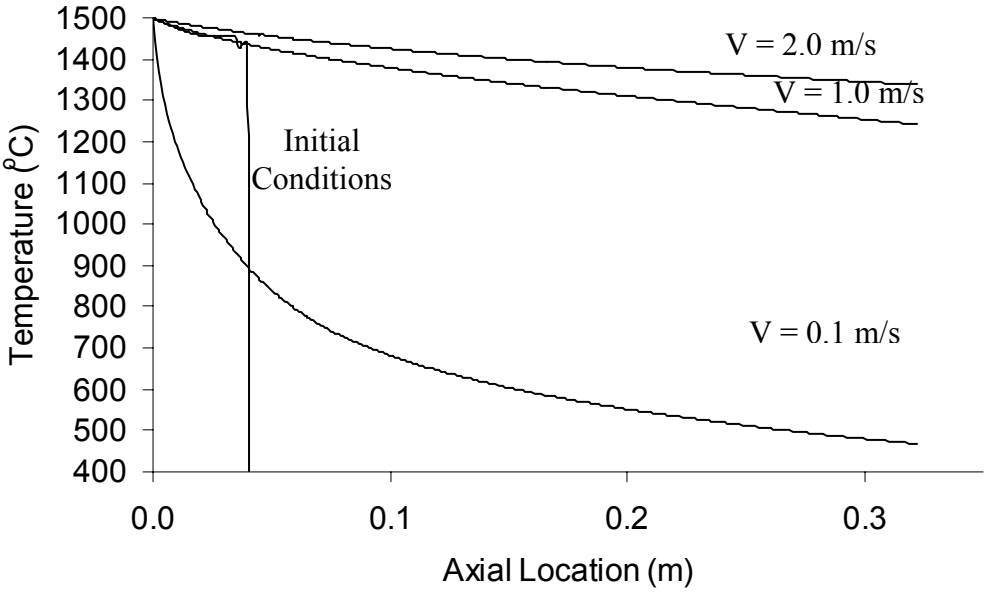

Figure 4.30 Examination of the impact of initial filling velocity on the cooling of the melt. Mold preheating temperature = 400 ^{o}C. h = 2000 W/m^{2}K

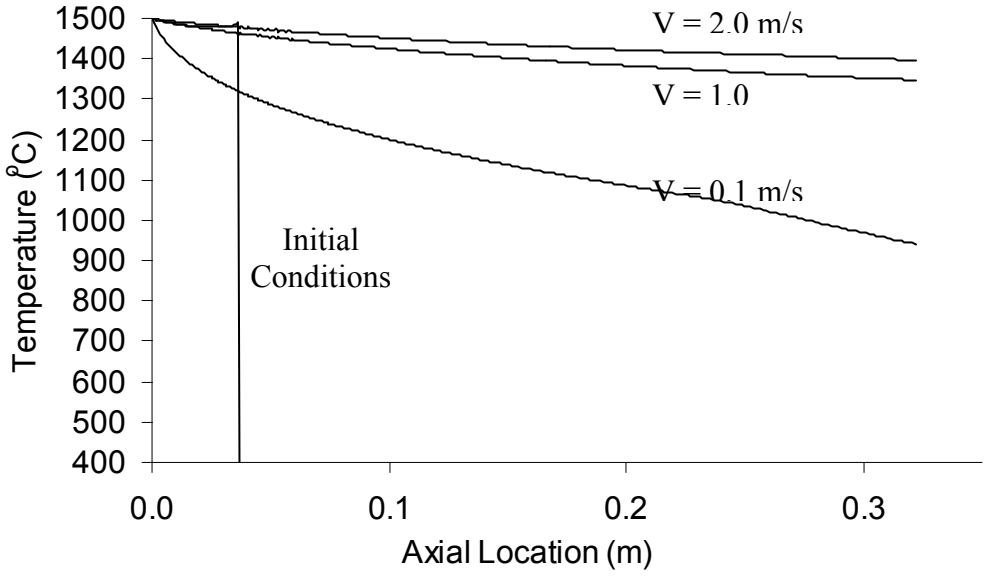

Figure 4.31 Examination of the impact of initial filling velocity on the cooling of the melt. Mold preheating temperature = 800 ^{o}C. h = 2000 W/m^{2}K

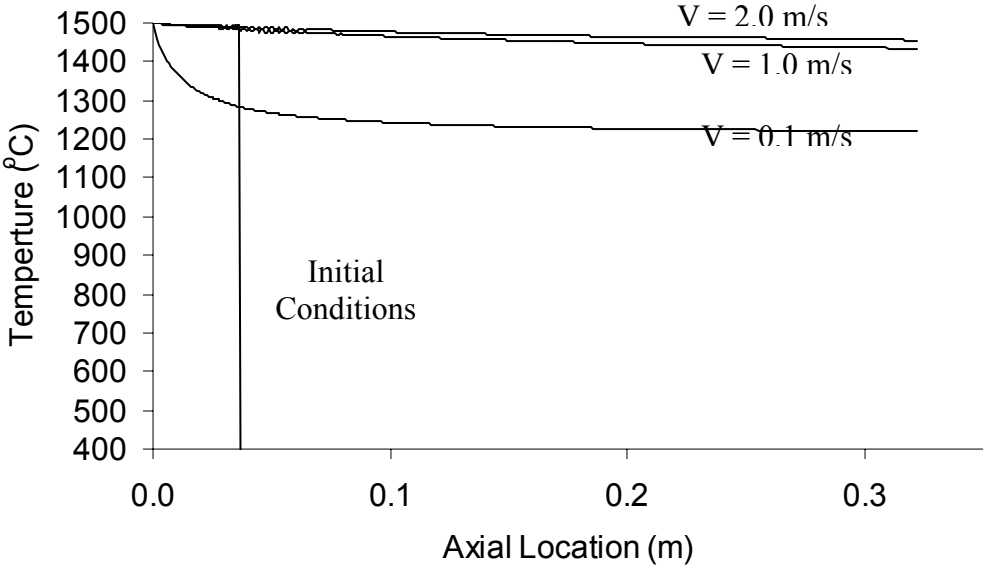

Figure 4.32 Examination of the impact of initial filling velocity on the cooling of the melt. Mold preheating temperature = 1200 ^{o}C. h = 2000 W/m^{2}K

4.1.5 Impact Of The Heat Transfer Coefficient On The Cooling Of The Melt

Figures 4.33 through 4.35 show the impact of the assumed heat transfer coefficient on the cooling of the melt. Depending on the theoretical research, the interfacial heat transfer coefficient is the most import factor affecting the heat transfer into the molds. The results clearly show this trend. The effect of higher heat transfer rate will obvious during lower filling velocity. The effect of mold preheating temperature can also be found. Lower mold temperature increases the heat transfer into the molds.

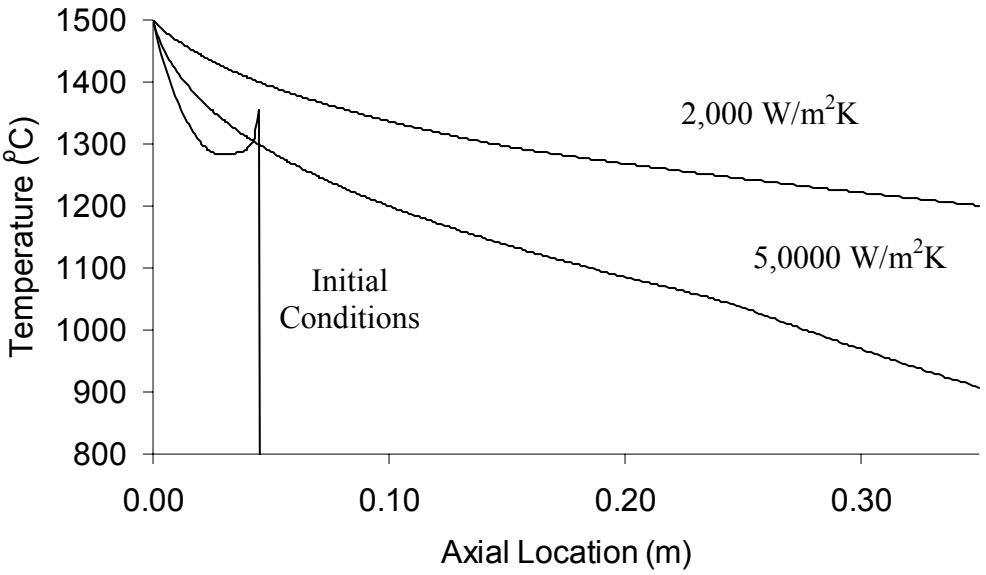

Figure 4.33 Examination of the impact of heat transfer coefficient on the cooling of the melt. Copper mold preheating temperature = 800 ^{o}C with 0.1 m/s initial velocity.

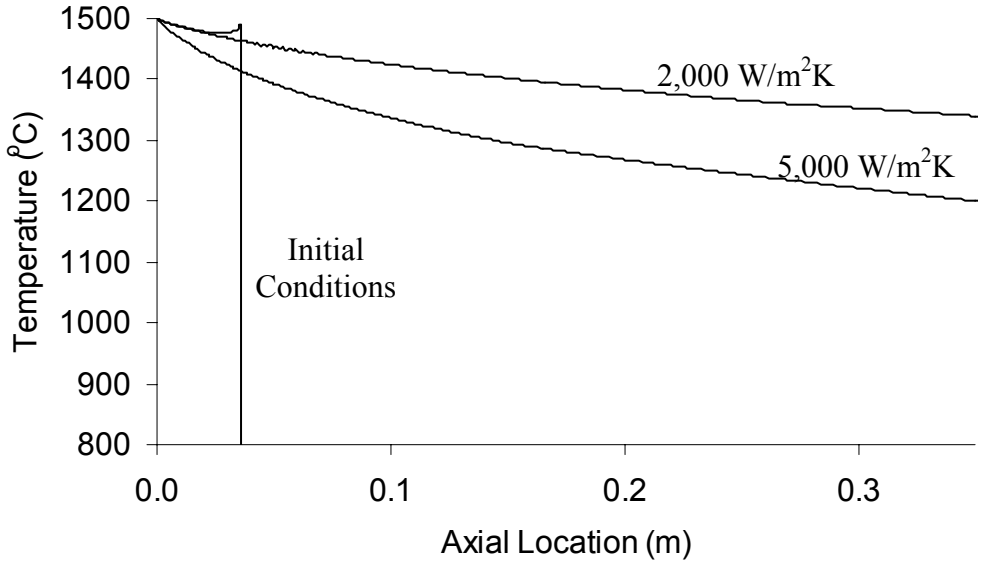

Figure 4.34 Examination of the impact of heat transfer coefficient on the cooling of the melt. Copper mold preheating temperature = 800 ^{o}C with 1.0 m/s initial velocity.

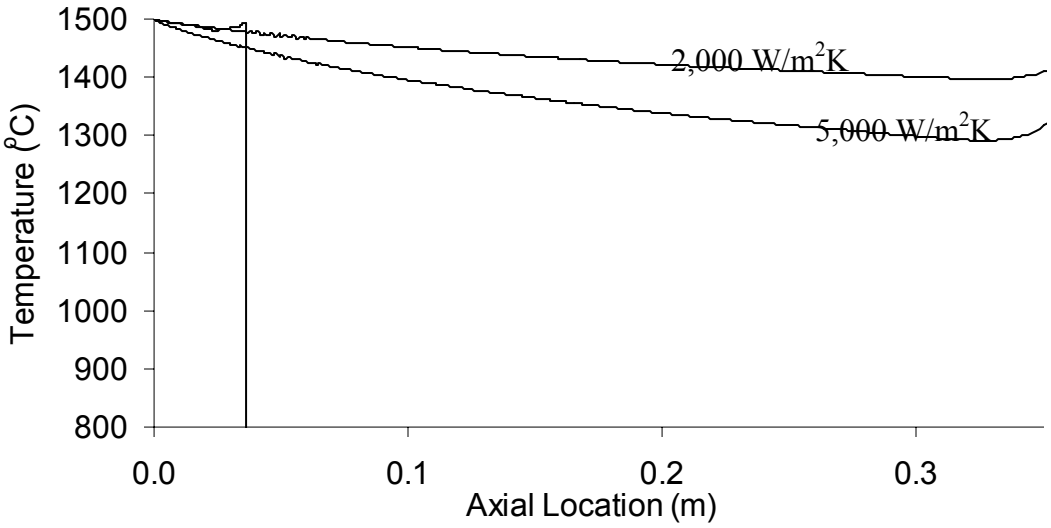

Figure 4.35 Examination of the impact of heat transfer coefficient on the cooling of the melt. Copper mold preheating temperature = 800 ^{o}C with 2.0 m/s initial velocity.

4.2 Temperature Profile For Quartz Molds

Figures 4.36 through 4.41 show the impact of different mold materials on the cooling of the melt. Heat transfer into the mold is faster using copper mold compared to quartz. The effect becomes more obvious during lower filling velocity. A lower heat transfer coefficient decreases the velocity of the heat transfer into the molds.

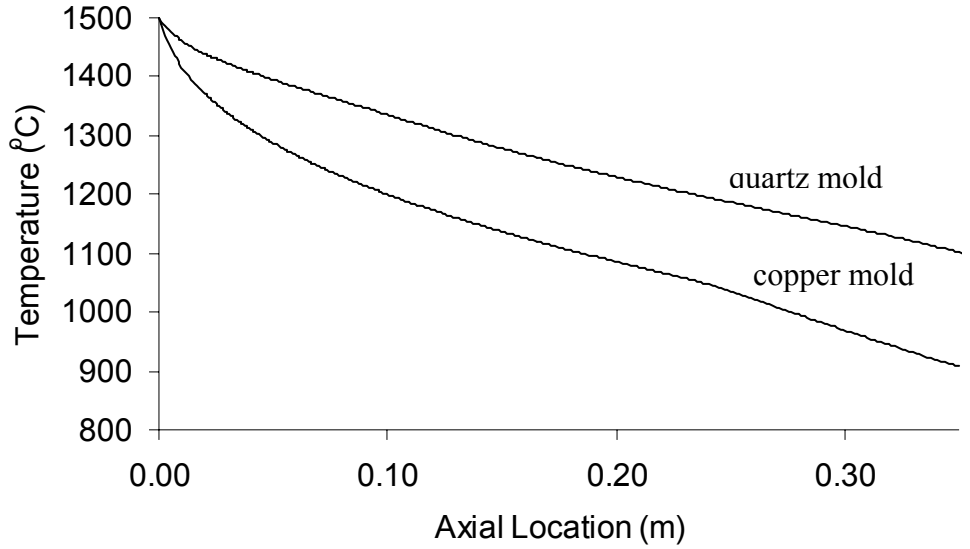

Figure 4.36 Examination of the impact of mold materials on the cooling of the melt. 2000 W/m^{2}K heat transfer coefficient, 0.1 m/s initial filling velocity and 800 ^{o}C mold preheating temperature .

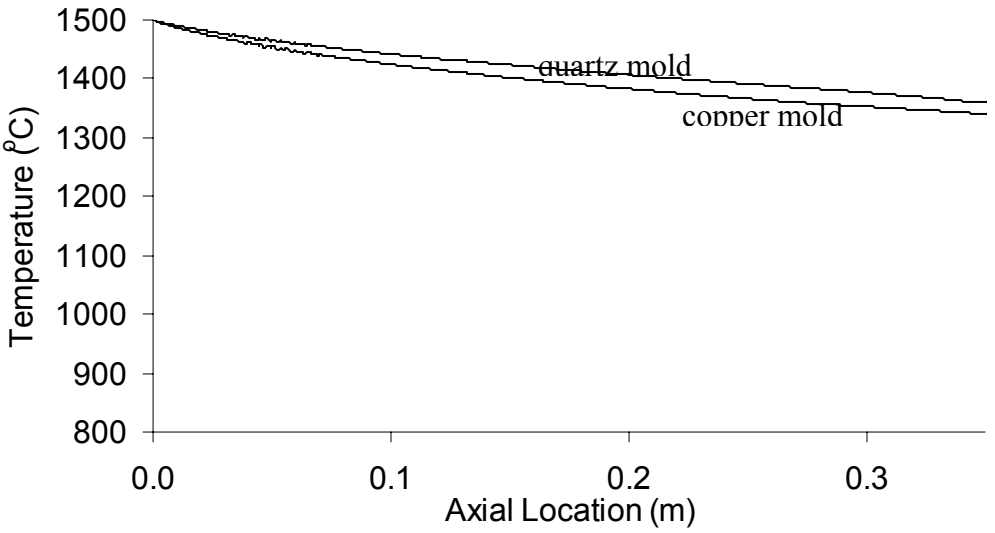

Figure 4.37 Examination of the impact of mold materials on the cooling of the melt. 2000 W/m^{2}K heat transfer coefficient, 1.0 m/s initial filling velocity and 800 ^{o}C mold preheating temperature .

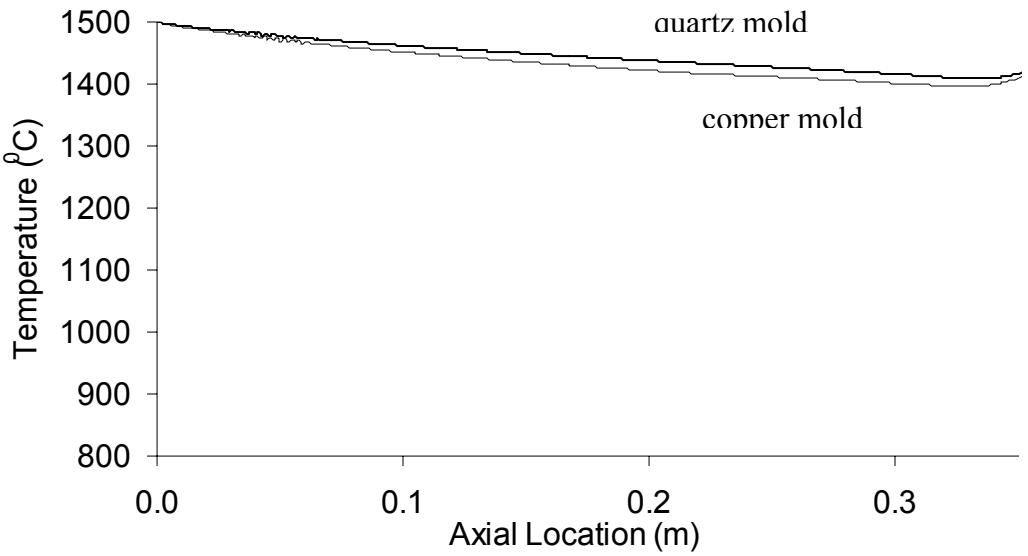

Figure 4.38 Examination of the impact of mold materials on the cooling of the melt. 2000 W/m^{2}K heat transfer coefficient, 2.0 m/s initial filling velocity and 800 ^{o}C preheating temperature.

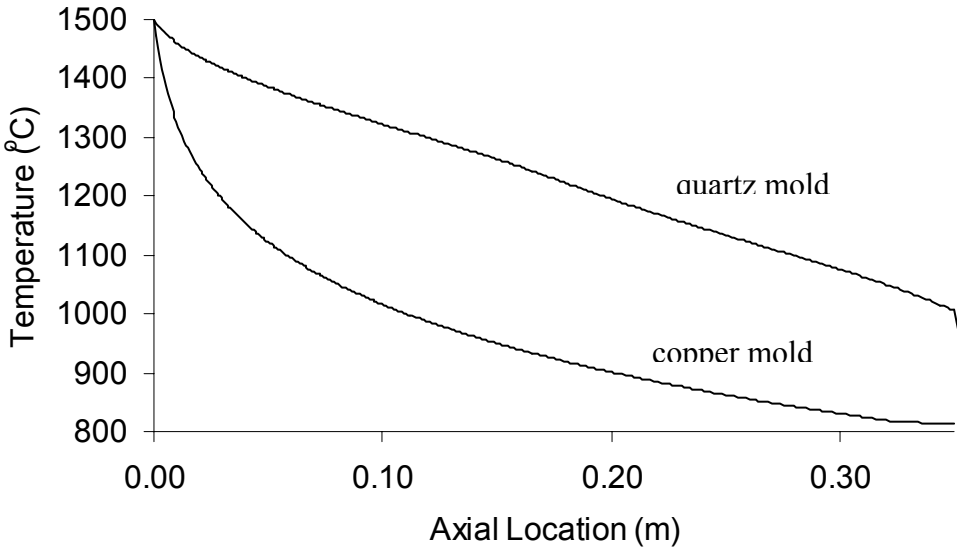

Figure 4.39 Examination of the impact of mold materials on the cooling of the melt. 5000 W/m^{2}K heat transfer coefficient, 0.1 m/s initial filling velocity and 800 ^{o}C mold preheating temperature.

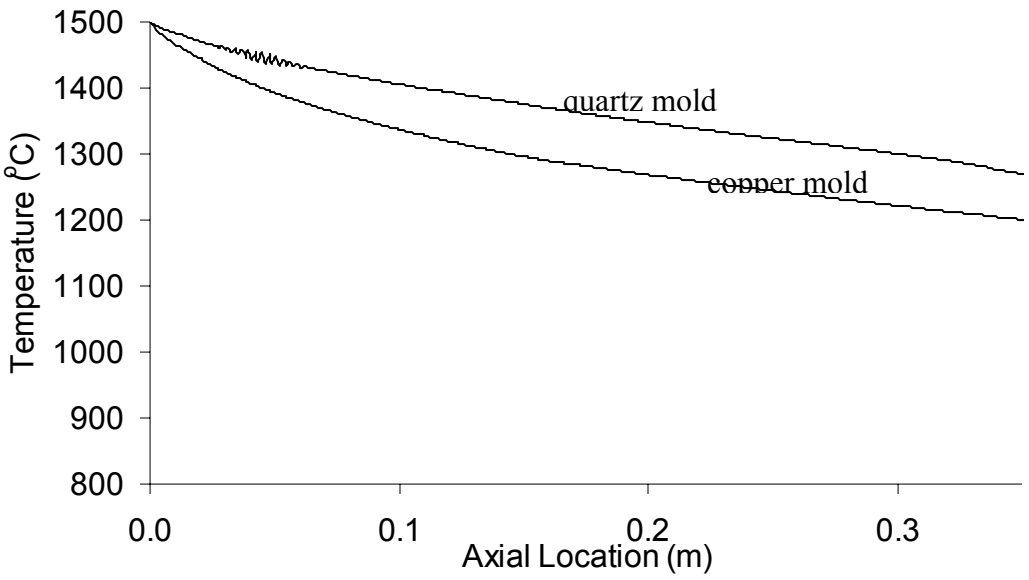

Figure 4.40 Examination of the impact of mold materials on the cooling of the melt. 5000 W/m^{2}K heat transfer coefficient, 1.0 m/s initial filling velocity and 800 ^{o}C mold preheating temperature.

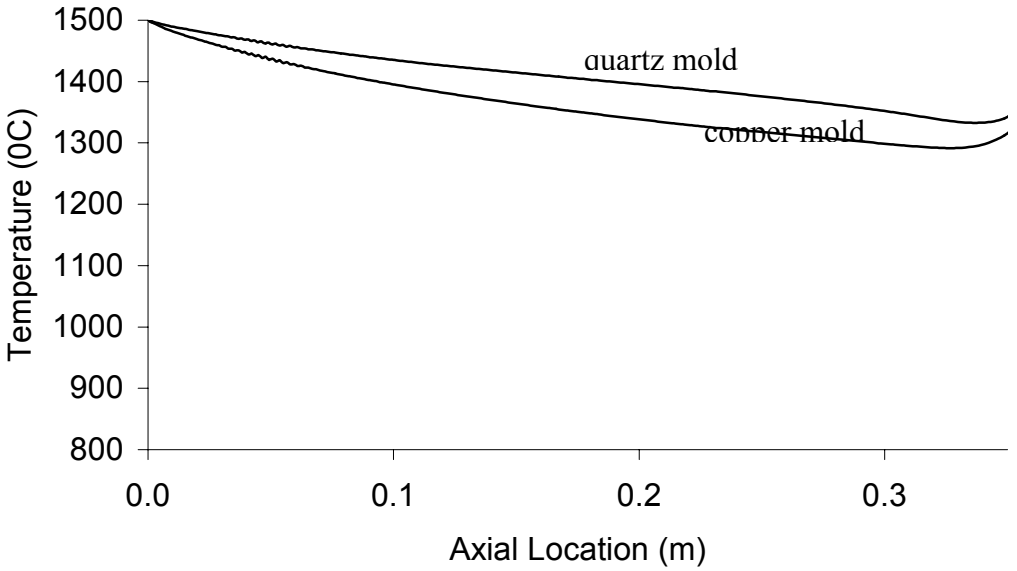

Figure 4.41 Examination of the impact of mold materials on the cooling of the melt. 5000 W/m^{2}K heat transfer coefficient, 2.0 m/s initial filling velocity and 800 ^{0}C mold preheating temperature.

CHAPTER 5

CONCLUSIONS

After considering the heating mechanisms, casting issues, crucible design and issues related to the mass transport of americium, the Induction Skull Melting concept was selected for casting fuel pins containing low vapor pressure materials (americium). The furnace includes a “lid” on the crucible region, “chill” molds, and resistance heaters to preheat the molds. The finite element commercial software (FIDAP) was used to simulate the flow of the melt into the molds, heat transfer into the molds, and impact of process parameters on the formation of the fuel rod. Factors, such as initial filling velocity, mold preheating temperature, heat transfer coefficient and mold material, are considered during the simulation. As shown in simulated results, mold materials, selected as copper and quartz, affect the heat transfer into the molds slightly. Meanwhile, changing mold preheating heating temperature had certain effect on the heat transfer into the molds. However, changing the heat transfer coefficient affected the heat transfer largely. This conclusion matches the theory discussed in the chapter 3.

REFERENCES

1. Dynamic Analysis of An overhead Crane Carrying A Canister By Finite Element Method –Musukula, University of Nevada, Las Vegas, 1993.
2. http://apt.lanl.gov/atw/index.html, (March 21, 2002).
3. http://www.nuc.berkeley.edu/designs/ifr/ ,(Aril 4, 2002).
4. Compilation of Information on Modeling of Inductively Heated Cold Crucible Melters, D.L. Lessor, March 1996.
5. Injection casting of U-Zr_Mn, surrogate alloy for U-Pu-Zr-Am-Np, C.L., Journal of Nuclear Materials 224(1995) 305-306.
6. The Induct slag Melting Process, P.G. Clites, (Bulletin/United States Department of the Interior, Bureau of Mines, 673), TN686.5.E45c57 1982.
7. Induction Skull Melting of Titanium Aluminides, P.G. Breig and S.W. Scott, the Duriron Company, Inc. 1989.
8. J. Szekely, J. McKelliget, and M. Choudhary, “Heat-transfer fluid flow and bath circulation in electric-arc furnace and dc plasma furnace”, Metals Society, Department of Material Science and Engineering, Massachusetts Institute of Technology, Cambridge, Mass., USA, 1982
9. Hazardous waste & Hazardous materials, Volume 11, Number 1, 1994.
10. The ABB DC arc furnace: Past, present, future, S.E. Stenkvist (ABB Process Automation), June 1992.

11. A Simplified Thermal Analysis of an Inductively Heated Casting Furnace, Randy Clarksean and Charles Solbrig, ASME Heat Transfer Division, Vol. 317-1, pp. 433-441.
12. Crucible for Induction Melting, Wilfried Guy, Kelsterbach, Germany, July, 1995.
13. Crucible for The Inductively Melting of Metals, Matthias Blum, Bodingen Wilfried Goy, Kelsterbach, Frauz Hage, Germany, Oct., 1996.
14. Cold Crucible Type Levitation Melting of Reactive Metals, A. Fukuzawa Chemical Processing Division .
15. The Further Development of the Semilevitation Melting Technique for The Production of Casting in Reactive Alloys, R A Harding and X R Zhu.
16. Innovative Method for Casting Steel Armorplate, Turnere, P.C and Jeffery S. Hansen, Washington, D.C., US Dept. of the Interior, Bureau of Mines, 1993
17. http://www.tms.org/pubs/journals/JOM/0201/cross/Cross-0201/.html, (Sep.20, 2001), The Multiphysics Modeling of Solidification and Melting Processes.
18. Thomas, B.G. "Casting Process Simulation and Visualization: A JOM-e Perspective," Journal of Metals, 54:1, 20-21, Jan. 2002.
19. C. Pequet and M. Rappaz, "Modeling of Porosity Formation during the Solidification of Al. Alloys Using a Mushy Zone Refinement Method," *Modeling of Casting, Welding and Advanced Solidification Processes IX,* ed. R. Sahm, N. Hansen, and G. Conley (Aachen, Germany: Shaker Verlag, 2000), pp. 71-79.
20. Zenger, D.C & Boothroyd, G., Selection of manufacturing processed and materials for component parts, Proceedings of 4th International Conference on Product Design for Manufacture and Assembly, Rhode Island, June 1989.

21. Allen, A.J. & Swift, K. G., Manufacturing process selection and costing system, Int. J. Adv. Manuf. Tech., 6, 205-215, 1991
22. Cook, R. D., Malkus, D.S. and Plesha, M.E., “Concepts and applications of finite element analysis”, John Wiley & Sons, New York, 1989, Third edition.
23. Hirt, C.W. and Nichols, B.D., "Volume of Fluid (VOF) Method for the Dynamics of Free Boundaries," Journal of Computational Physics, 201, 1981.
24. S.Kvicinsky, F. Longatte, J.-L. Kueny and F. Avellan, “Free Surface Flows: Experimental Validation of Volume of Fluid (VOF) Method in the Plane Wall Case”, Proceedings of the 3rd ASME/JSME Joint Fluids Engineering Conference, July 18-23 1999, San Francisco, California.
25. Nichols, B.D. and Hirt, C.W., "Methods for Calculating Multi-Dimensional, Transient Free Surface Flows Past Bodies," Proc. First Intern. Conf. Num. Ship Hydrodynamics, Gaithersburg, ML, Oct. 20-23, 1975.
26. C.A. Santos, J.M.V. Quaresma, A. Garcia, “Determination of transient interfacial heat transfer coefficient in chill mold castings”, Journal of Alloys and Compounds, 319 (2001), 174-186.
27. F. Michel, P.R. Louchez, F.H. Samuel, “ Heat Transfer Coefficient During Solidification of Al-Si Alloys: Effects of Mold Temperature, Coating Type and Thickness”, University du Quebec a Chicoutimi, Chicoutimi, Quebec, Canada

REFERENCES

1. Dynamic Analysis of An overhead Crane Carrying A Canister By Finite Element Method –Musukula, University of Nevada, Las Vegas, 1993.
2. http://apt.lanl.gov/atw/index.html, (March 21, 2002).
3. http://www.nuc.berkeley.edu/designs/ifr/ ,(Aril 4, 2002).
4. Compilation of Information on Modeling of Inductively Heated Cold Crucible Melters, D.L. Lessor, March 1996.
5. Injection casting of U-Zr_Mn, surrogate alloy for U-Pu-Zr-Am-Np, C.L., Journal of Nuclear Materials 224(1995) 305-306.
6. The Induct slag Melting Process, P.G. Clites, (Bulletin/United States Department of the Interior, Bureau of Mines, 673), TN686.5.E45C57 1982.
7. Induction Skull Melting of Titanium Aluminides, P.G. Breig and S.W. Scott, the Duriron Company, Inc. 1989.
8. J. Szekely, J. McKelliget, and M. Choudhary, "Heat-transfer fluid flow and bath circulation in electric-arc furnace and dc plasma furnace", Metals Society, Department of Material Science and Engineering, Massachusetts Institute of Technology, Cambridge, Mass., USA, 1982
9. Hazardous waste & Hazardous materials, Volume 11, Number 1, 1994.
10. The ABB DC arc furnace: Past, present, future, S.E. Stenkvist (ABB Process Automation), June 1992.

NOMENCLATURE

u	velocity of the melt flow (m/s)
ρ	density of the melt flow (Kg/m^3)
p	pressure using to fill the melt flow (N/m^2)
T	temperature of the flow (^0C)
T_0	reference temperature (^0C)
g	local acceleration (m/s^2)
μ	viscosity of the melt material ($N \cdot s/m^2$)
C_p	specific heat of the melt flow ($J/Kg \cdot K$)
k	thermal conductivity ($W/m \cdot K$)
T_{mt}	temperature of molds (^0C)
K_{mt}	thermal conductivity of the molds ($W/m \cdot K$)
F	an indicator function to represent the fluid volume (m^3)
f_i	value to represent the filled state, 1 means a filled state, 0 means a empty state
V_i	volume of the fluid (m^3)
h	average metal –mold interfacial heat transfer coefficient (W/m^2K)
q	average heat flux across the interface (W)
∇	gradient operator
$\nabla \cdot$	divergence operator

Subscripts

0	reference state
p	pressure
l	liquid state
s	solid state
m	melting point
n	normal direction of the interface
mt	mold
i	any state between solid and liquid including pure solid and liquid
1M	mold surface
1C	casting surface

APPENDIX I

AMERICIUM PROPERTIES

Historical: Americium, element 95, was discovered in 1944-45 by Seaborg et al. [1] at the Metallurgical Laboratory of the University of Chicago. The reaction used was:

$$^{239}Pu\,(n,\gamma)\,^{240}Pu\,(n,\gamma)\,^{241}Pu \xrightarrow[14\ yr]{\beta^-} {}^{241}Am$$

During all the isotopes of americium from ^{237}Am to ^{246}Am, only ^{243}Am (half-life = 7600 years) and ^{241}Am (half-life = 433 years) are sufficiently long lived to permit accurate property studies and are the most important and the most useful for chemical research.

Metal Preparation [2]: Americium metal has been prepared by the following methods:

1. Reduction of AmF_3 with barium (or lithium) metal
2. Reduction of AmO_2 with lanthanum metal
3. Bomb reduction of AmF_4 with calcium metal
4. Thermal decomposition of Pt_5Am

Allotropy [3]:Americium metal is silvery, ductile, non-magnetic and very malleable. There are three well-established forms of americium metal:

1. phase: double hexagonal close-packed structure
2. β phase: body-centered structure
3. γ phase: face-centered cubic structure

Thermodynamics of Americium Metal Transitions

Transition	T(K)	ΔH_t(KCal·mol^{-1})	ΔS(Cal·K^{-1}·mol^{-1})
$\alpha \rightarrow \beta$	923±50	0.185	0.2
$\beta \rightarrow \gamma$	1349±5	1.400	1.04
$\gamma \rightarrow$liq	1449±3	3.440	2.37

Selected Properties of Americium Metal

Property	Value
Atomic number	95
Density	13.671 g/cm^{-3}
High-pressure structures	0-5 GPa, dhcp 5-10 GPa, fcc 10-15 Gpa, double body-centered monoclinic >15 Gpa, orthorhombic –uranium or monoclinic (α-uranium alloys)
Melting point	1176, 1173, or 1170^{0}C
Boiling point	2067^{0}C or 2284^{0}C
Vapor pressure	log(p/atm) = (6.5780±.046)-(14315±55)/T at 990-1358K
Heat of vaporization at boiling point	230.2KJmol^{-1}(calc.)
Entropy of vaporization at boiling point	100.8 J K^{-1}mol^{-1}
Heat of fusion	14.4KJmol^{-1}

For the α–phase we estimate the following value:

$$C_p(Am,\alpha) = 5.294 + (2.883*10^{-3})T + (0.272*10^{-6})T^2$$

For the β–phase we estimate the following value:

$$C_p(Am,\beta) = 5.196 + (1.964*10^{-3})T + (7.38*10^{-7})T^2$$

Thermodynamic Quantities For Americium Ions [4]:

Ion	ΔH_f^0(298K), KCal·mol^{-1}	ΔG_f^0(298K) KCal·mol^{-1}	S^0(298K) Cal·K^1·mol^{-1}	Hydration enthalpy and entropy	
				$-\Delta H_h$, KCal·mol^{-1}	$-S_h$, Cal·K^1·mol^{-1}
Am^{3+}·aq	147.4±0.3	143.2±0.9	48±3	832	91.8
Am^{4+}·aq	103.4±2.6	89.2±2.4	97±5	1635	128
AmO_2^{+}·aq	192.4±1.1	177.7±1.3	3±2		
AmO_2^{2+}·aq	155.8±0.5	141.0±0.8	19±2		

1. Seaborg, G. T., Katz, J. J., and Manning, W. M. (eds) (1949) *The Transuranium Elements: Research Paper*, Natl Nucl. En. Ser., Div. IV, 14B, McGraw-Hill, New York
2. Joseph J. Katz, Glenn T. Seaborg and Lester R. Morss, "The chemistry of the actinide elements", second edition, volume 2
3. F.L. Oetting, M.H. Rand and R.J. (1976) *The Chemical Thermodynamics of Actinides Elements and Compounds* (Part1: The actinides elements), International Atomic Energy Agency, Vienna
4. Schulz, Wallace W., "The Chemistry of Americium"

Decay heat from ^{241}Am:

- $t_{1/2}$ = 432 years
- $\lambda = \frac{\ln 2}{t_{\frac{1}{2}}} = \frac{0.693}{432 \times 365 \times 24 \times 3600} \cong 0.51 \times 10^{-10}\, s^{-1}$
- $\dot{R} = \lambda NE = (0.51 \times 10^{-10}\ \frac{dis}{s}) \cdot (\frac{13.6 \frac{g}{cm^3} \times 6.023 \times 10^{23}\ mol^{-1}}{241\ \frac{g}{mold}}) \cdot (4\ \frac{\mu ev}{dis})$
- $= (69.36 \times 10^{11}\ \frac{\mu ev}{s - cm^{-3}}) \cdot (1.602 \times 10^{-7}\ \frac{J}{\mu ev})$
  $= 1.11 \times 10^{6}\ \frac{W}{cm^3}$

APPENDIX II

INPUT FILE

```
//slip_6.in
//This is the mesh file for our model. Here shows the geometry data and //the mesh
informaiton
default load "e:\fluent.inc\GAMBIT.ini"
undo begingroup
vertex create coordinates 0 0 0
vertex create coordinates 0 0.004 0
vertex create coordinates 0 0.008 0
vertex create coordinates 0.02 0 0
vertex create coordinates 0.02 0.004 0
vertex create coordinates 0.02 0.008 0
vertex create coordinates 0.5 0 0
vertex create coordinates 0.5 0.004 0
vertex create coordinates 0.5 0.008 0
/
vertex create coordinates 0 0.0041 0
vertex create coordinates 0.02 0.0041 0
vertex create coordinates 0.5 0.0041 0
undo endgroup
/
edge create straight "vertex.1" "vertex.4"
edge create straight "vertex.2" "vertex.5"
edge create straight "vertex.10" "vertex.11"
edge create straight "vertex.3" "vertex.6"
edge create straight "vertex.1" "vertex.2"
edge create straight "vertex.10" "vertex.3"
edge create straight "vertex.4" "vertex.5"
edge create straight "vertex.11" "vertex.6"
edge create straight "vertex.4" "vertex.7"
edge create straight "vertex.5" "vertex.8"
edge create straight "vertex.11" "vertex.12"
edge create straight "vertex.6" "vertex.9"
edge create straight "vertex.7" "vertex.8"
edge create straight "vertex.12" "vertex.9"
face create wireframe "edge.1" "edge.5" "edge.2" "edge.7" real
face create wireframe "edge.3" "edge.6" "edge.4" "edge.8" real
```

```
face create wireframe "edge.9" "edge.7" "edge.10" "edge.13" real
face create wireframe "edge.11" "edge.8" "edge.12" "edge.14" real
undo begingroup
edge picklink "edge.13" "edge.7" "edge.5"
edge mesh "edge.5" "edge.7" "edge.13" successive ratio1 1.0 intervals 12
undo endgroup
undo begingroup
edge picklink "edge.14" "edge.8" "edge.6"
edge mesh "edge.6" "edge.8" "edge.14" successive ratio1 1.0 intervals 12
undo endgroup
undo begingroup
edge picklink "edge.4" "edge.3" "edge.2" "edge.1"
edge mesh "edge.1" "edge.2" "edge.3" "edge.4" successive ratio1 1.0 intervals \
  24
undo endgroup
undo begingroup
edge picklink "edge.12" "edge.11" "edge.10" "edge.9"
edge mesh "edge.9" "edge.10" "edge.11" "edge.12" successive ratio1 1.003 \
  intervals 400
undo endgroup
face mesh "face.1" "face.3" "face.4" "face.2" map size 1
/
physics create "inlet" btype "PLOT" edge "edge.5"
physics create "l_end" btype "PLOT" edge "edge.6"
physics create "wall_1" btype "CONVECTION" edge "edge.2"
physics create "wall_2" btype "CONVECTION" edge "edge.3"
physics create "center" btype "PLOT" edge "edge.1" "edge.9"
physics create "interface" btype "CONVECTION" edge "edge.10"
physics create "interface2" btype "CONVECTION" edge "edge.11"
physics create "outer_rod" btype "PLOT" edge "edge.4" "edge.12"
physics create "outlet" btype "PLOT" edge "edge.13"
physics create "r_end" btype "PLOT" edge "edge.14"
physics create "flow2" ctype "FLUID" face "face.3"
physics create "flow1" ctype "FLUID" face "face.1"
physics create "mold" ctype "SOLID" face "face.2" "face.4"
export fidap "slip_6.mesh"
/



//slip_6.read
// This is the file shows how do we define the problem, all the boundary and initial
//conditions, how to solve .
/
```

```
/        CONVERSION OF NEUTRAL FILE TO FIDAP Database
/
FICONV( NEUTRAL )
INPUT( FILE="slip_6.mesh" )
OUTPUT( DELETE )
END
/
TITLE
SLIP; 0.5 m length; mold 400 C; Re~2500
/
FIPREP
/
/   PROBLEM SETUP
/
PROBLEM (TRANSIENT, NONLINEAR, ENERGY, AXI-SYMMETRIC)
FILLING (FILL, COURANT = 0.5, NOSUBCYCLE, 1PROP = "melt")
/
/ suggested by FIDAP folks
/
PRESSURE( MIXED = 1.E-8, DISC )
/
OPTIONS( UPWINDING )
/
EXECUTION( NEWJOB )
PRINTOUT( NONE )
DATAPRINT( CONTROL )
/
/        CONTINUUM ENTITIES
/
ENTITY ( NAME = "flow2", FLUID, PROPERTY = "melt", MFCNV = "fill_ht" )
ENTITY ( NAME = "flow1", FLUID, PROPERTY = "melt", MFCNV = "fill_ht" )
ENTITY ( NAME = "mold", SOLID, PROPERTY = "quartz glass" )
/
/        BOUNDARY ENTITIES
/
ENTITY ( NAME = "inlet", PLOT )
ENTITY ( NAME = "outlet", PLOT )
/
ENTITY ( NAME = "center", PLOT )
/
ENTITY ( NAME = "outer_rod", ATTACH = "mold", PLOT )
ENTITY ( NAME = "l_end", ATTACH = "mold", PLOT )
ENTITY ( NAME = "r_end", ATTACH = "mold", PLOT )
/
```

```
ENTITY ( NAME ="interface", ATTACH="flow2", CONVECTIVE,
  SLAVE = "interface2", MCNV = "gap_h" )
ENTITY ( NAME ="wall_1", ATTACH="flow1", CONVECTIVE,
  SLAVE = "wall_2", MCNV = "gap_h" )
ENTITY ( NAME ="interface2", ATTACH="mold", CONVECTIVE,
  SLAVE = "interface", MCNV = "gap_h" )
ENTITY ( NAME ="wall_2", ATTACH="mold", CONVECTIVE,
  SLAVE = "wall_1", MCNV = "gap_h" )
/
/
/         SOLUTION PARAMETERS
/
SOLUTION(SEGREGATED=100,CG, CGS, PRECON=21, NCGC=1.0E-6,
SCGC = 1.0E-6 )
/
POSTPROCESS(NBLOCK=1)
1,20001,50
TIME(BACKWARD,NSTEP=5000,DT=0.00100, TEND=5.0, FIXED,
INCMAX = 1.2, WINDOW = 0.20, UCHAR = 4  )
/
CLIPPING ( MAXIMUM )
0 0 0 0 1500.0 0
CLIPPING ( MINIMUM )
0 0 0 0 1000.0 0
/
/
/         MATERIAL PROPERTIES
/
/ Partial list of Material Properties data
/
DENSITY( SET = "melt", CONSTANT = 19800. )
/VISCOSITY( SET = "melt", CONSTANT = 5.5E-3 )
VISCOSITY( SET = "melt", CONSTANT = 0.10 )
CONDUCTIVITY( SET = "melt", CONSTANT = 6 )
/
/ estimated from Zirconium properties
/
SPECIFICHEAT( SET = "melt", CONSTANT = 150.0 )
/
/ ++++++++++++++
/
DENSITY( SET = "quartz glass", CONSTANT = 2200 )
CONDUCTIVITY( SET = "quartz glass", CONSTANT = 1.4 )
SPECIFICHEAT( SET = "quartz glass", CONSTANT = 670 )
```

```
/
/         INITIAL AND BOUNDARY CONDITIONS
/
ICNODE( FILL , CONSTANT = 1, ENTITY = "flow1" )
ICNODE( FILL , CONSTANT = 1, ENTITY = "interface" )
ICNODE( FILL , CONSTANT = 1, ENTITY = "wall_1" )
/
BCNODE( FILL, CONSTANT = 1, ENTITY = "inlet" )
/
BCNODE( URC, CONSTANT = 0, ENTITY = "inlet" )
/
/
BCNODE( TEMP, CONSTANT = 1500.0, ENTITY = "inlet" )
ICNODE( TEMP , CONSTANT = 1500, ENTITY = "flow1" )
ICNODE( TEMP, CONSTANT = 400.0, ENTITY = "mold" )
/
HTRANSFER ( SET = "gap_h", CONSTANT = 2000.0)
HTRANSFER ( SET = "fill_ht", CONSTANT = 0.0)
/
BCNODE (URC, ZERO, ENTITY = "wall_1" )
BCNODE (URC, ZERO, ENTITY = "interface" )
BCNODE (UZC, FREE, ENTITY = "interface" )
BCNODE (UZC, FREE, ENTITY = "wall_1" )
/
BCNODE( UZC, CONSTANT = 0.1, ENTITY = "inlet" )
/
BCNODE( URC , ZERO , ENTITY = "center" )
BCFLUX( HEAT , CONSTANT = 0.00 , ENTITY = "center" )
BCFLUX( HEAT , CONSTANT = 0.00 , ENTITY = "l_end" )
BCFLUX( HEAT , CONSTANT = 0.00 , ENTITY = "r_end" )
BCFLUX( HEAT , CONSTANT = 0.00 , ENTITY = "outer_rod" )
/
/
END
/
CREATE( FISOLV )
```

VITA

Graduate College
University of Nevada, Las Vegas

Xiaolong Wu

Local Address:
4248 Chatham Cir #3
Las Vegas, NV 89119

Home Address:
#28 ChengLingZhung, HeDong District
Tianjing, China

Degrees:
Bachelor of Science, Mechanical Engineering, 1998
Nanjing University of Aeronautics & Astronautics

Thesis Title: Design and Analysis for Melt Casting Metallic Fuel Pins Incorporating Volatile Actinides

Thesis Examination Committee:
Chairperson, Dr. Darrell W. Pepper, Ph.D.
Chairperson, Dr. Yitung Chen, Ph.D
Committee Member, Dr. Robert Boehm, Ph.D.
Committee Member, Dr. William Cullbreth, Ph.D.
Committee Member, Dr. Jichun Li, Ph.D.